
Text-Guided Data Attribution: Attributing the Influence of Simplicity Bias to Dataset

Anonymous Author(s)

Affiliation

Address

email

Abstract

1 The effectiveness of deep learning models heavily relies on the quality and diversity of their training data. However, datasets collected from different sources
2 often introduce simplicity biases, where a models rely on easily learnable but non-predictive (spurious) features for its predictions. While existing debiasing
3 techniques focus on model robustness, they leave the data untouched. Further,
4 they require manual group annotation of the entire training data or changes in
5 training strategy, which are often constrained by privacy, regulatory, or proprietary
6 constraints. As data becomes increasingly valuable, identifying and mitigating
7 bias directly at the data level has gained importance. Recently, data attribution
8 has emerged as a promising tool for uncovering issues in training data, yet its
9 vulnerability to simplicity bias has received limited attention. In this work, we
10 propose a novel data deletion framework that combines Neural Tangent Kernel
11 (NTK)-based data attribution with textual descriptions of bias to identify and re-
12 move training samples that do not significantly affect model performance. We first
13 demonstrate that NTK-based data attribution methods can themselves be influenced
14 by spurious features. Subsequently, to mitigate this, we use available metadata
15 or, when unavailable, a vision-language model, to annotate a small validation set
16 and extract a textual description of the bias. Based on this description, we identify
17 training samples that are semantically aligned with the spurious feature and exhibit
18 high detrimental attribution scores. Removing these samples from the training
19 data and retraining the model on the new training set improves its performance.
20 Our approach achieves better average and worst-group accuracy, outperforming
21 existing attribution-based baselines.
22
23

24 1 Introduction

25 The success of deep learning models is strongly influenced by the quality and quantity of the dataset
26 used for training [1–4]. These data are often collected via web scraping [5, 6], and external data
27 providers [7, 8]. However, such datasets can inadvertently contain illegal content [9] and can
28 encode negative societal biases [10, 11] that can influence model performance. In addition, data
29 collected from such varied sources can introduce distributional shifts, where subpopulations with
30 specific features may be overrepresented or underrepresented in the training data compared to the test
31 data [12].

32 These imbalances can introduce simplicity bias [13–15] where the model, due to high correlations
33 between specific features and the prediction task, relies on simpler, non-robust (spurious) features
34 instead of learning predictive features for classification. Several methods have been proposed to handle
35 such biases in the model. However, instead of addressing the data as the fundamental source of bias,
36 they primarily focus on improving model robustness by reweighting the loss function [16], modifying

37 the training objective [17–19], and model fine-tuning [20]. While effective, they inadvertently modify
38 the standard training pipeline, which can increase the model’s susceptibility to adversarial attacks [21–
39 24], and could conflict with regulatory requirements, especially in safety-critical settings [25, 26],
40 which require adherence to a specific training regime for theoretical guarantees. Further, considering
41 the inherent proprietary value of data [27] and the monetary investment needed for collecting a new
42 dataset, it has become increasingly important to address these challenges at the data level.

43 A viable alternative in these scenarios could be to remove training samples containing spurious
44 features [28, 29, 11], by ensuring that these samples don’t hurt the overall performance of the model,
45 as in data attribution and Leave-One-Out (LOO) techniques [30–32]. Data attribution methods aim to
46 estimate a model’s performance when specific training samples are excluded, enabling the evaluation
47 of counterfactual scenarios—such as assessing the impact on test accuracy if certain subsets of
48 the training data were omitted [31, 33, 34]. However, many of these methods are computationally
49 expensive and can underperform in non-convex settings. Recent advancements in data attribution
50 methods, such as Trak [32], leverage neural tangent kernels (NTK) to enable scalable data attribution
51 for non-convex models [32]. However, the impact of spurious features on the data attribution scores
52 generated by such methods remains an open question.

53 In our work, we demonstrate (Proposition 1, Appendix J) that in the presence of data bias, methods
54 like Trak [32] can undervalue the attribution scores for training samples with spurious features [13–
55 15]. This misattribution can hinder the identification of detrimental samples, especially for methods
56 that rely solely on the magnitude of attribution scores [35, 31].

57 Motivated by these observations, we propose a two-stage strategy to mitigate the impact of spurious
58 features - (a) In the first stage, we focus on identifying such features within the dataset using available
59 meta-data or annotations generated by a vision language model. (b) In the second stage, we use
60 multimodal embeddings, such as CLIP [36] to learn a metric [37, 38] that identifies training examples
61 that are semantically similar to the spurious features identified in the first step and whose removal
62 can improve the model’s performance as per the attribution scores.

63 The spurious features in the first stage are identified using metadata wherever available. In cases where
64 metadata is unavailable, we utilize a vision-language model (VLM) to annotate a small validation
65 set with its respective attributes and their associated values that are likely to introduce simplicity
66 biases [39–41]. By evaluating the model’s performance on these attribute-value pairs and comparing
67 it to the overall performance on the validation dataset [42], we identify potential spurious features
68 and generate a corresponding textual description of these biases [43]. This textual representation
69 enables targeted data pruning and helps to mitigate the impact of spurious features without relying on
70 manual group annotations in the training dataset.

71 In summary, our contributions in this paper are as follows:

- 72 • We propose a novel data-centric approach that combines NTK-based data attribution methods
73 with textual descriptions of underlying bias to mitigate the impact of spurious features in
74 training datasets.
- 75 • We first theoretically demonstrate that NTK-based attribution scores can be influenced
76 by spurious features, which may limit the effectiveness of methods that rely solely on
77 these scores for data pruning. To overcome this limitation, we introduce a metric learning-
78 based data deletion strategy that selectively removes training samples aligned with textual
79 descriptions of spurious features and exhibiting low attribution scores.
- 80 • Our approach achieves up to a 4% gain in average accuracy, 18% in worst-group accuracy,
81 and a 50% improvement in class-level performance across various datasets. Additionally, it
82 outperforms NTK-based methods like Trak on average by 10.6% in worst-group accuracy
83 for different biased datasets.

84 2 Related Work

85 2.1 Data Attribution

86 Data attribution methods provide a framework to relate a model’s predictions to its training dataset
87 and have been used in a wide range of tasks, including model debugging and repair [44–47], subset
88 selection [33, 34, 48], group robustness [11] and removing poisoning attacks [49].

89 The idea of linking a model’s predictions to its training data has been studied for decades under various
90 names, including influence functions [50], regression analysis [51], and jackknife methods [52].
91 However, most of these early works focused on linear models and aimed to predict changes in the
92 optimal parameters when individual or groups of samples were excluded during the learning process.
93 Recent works have tried to extend influence function and jackknife-based attribution methods to
94 non-linear models and bigger datasets [30, 53, 54]. However, despite their promising predictive
95 capabilities, these methods often make strong assumptions of strong convexity and the existence of a
96 unique global solution, which are not applicable for neural networks [55]. Furthermore, Basu et al.
97 [56], Hammoudeh and Lowd [57] have demonstrated the fragile nature of methods like influence
98 functions across different architectures, showing that they sometimes fail basic sanity checks. Various
99 approaches have been proposed to address the limitations of influence functions, including gradient
100 agreement scoring [58], training models to predict attribution scores, as in DataModels [59], and
101 methods like Trak [32], which leverage concepts from the Neural Tangent Kernel (NTK) for data
102 attribution. Unlike other approaches, such as DataModels, Trak does not require training thousands of
103 models [32, 59] or tracking the loss changes over the entire training process, making it more efficient.
104 However, the impact of spurious features within the dataset on the data attribution method like Trak
105 remains largely unexplored.

106 2.2 Spurious Features and Simplicity Bias

107 Spurious features often arise from selection bias in the dataset [60], where, in the presence of
108 multiple hypotheses for prediction, the model tends to rely on the simplest feature [61, 14, 13]. This
109 preference can lead to suboptimal model performance, as it often ignores more robust and meaningful
110 features that are essential for generalization in real-world scenarios. Various methods have been
111 proposed to address spurious features in models. These include data augmentation techniques [62–
112 67], and learning strategies that change the training objectives to make the model robust to spurious
113 features [17, 68, 69, 19, 16, 70, 20]. However, many of these changes are restricted under the
114 regulatory policy for safety-critical applications [71–74], especially considering privacy concerns
115 associated with collecting datasets and model certification-based requirements [75, 76]. Recent
116 work has explored data deletion as a strategy for mitigating spurious features [28, 29, 11]. These
117 methods use group annotation of the dataset to remove random samples from majority groups [28,
118 29] or those with high detrimental attribution scores [11]. However, these methods often require
119 manual group annotation of training [28, 29] or validation data [11], which is costly and time-
120 consuming. Further, in real-world settings, where biases are identified post hoc after deployment
121 and evolve over time [77], generating such annotations is often impractical, and enforcing a balance
122 among different groups may result in excessive data removal from the majority group and can harm
123 generalization [29]. Our method circumvents these limitations by using text-guided data attribution
124 to efficiently remove harmful samples within a deletion budget, without relying on group labels or
125 hurting model performance. Further details on limitations and capabilities of existing methods are
126 discussed in Appendix E.

127 3 Proposed Method

128 3.1 Problem Definition

129 Consider a classification setting with a training dataset $\mathcal{D}_{\text{train}} = \{z_1, \dots, z_n\}$, where each sample
130 $z_i = (x_i, y_i)$, consisting of an input (x_i) and associated class label (y_i) and a validation dataset,
131 $\mathcal{D}_{\text{val}} = \{v_1, \dots, v_m\}$ with validation samples $v_j = (x_j, y_j)$. The training dataset ($\mathcal{D}_{\text{train}}$) is used to
132 train a neural network with optimal parameters $\theta^*(\mathcal{D}_{\text{train}})$. Additionally, we assume that $|\mathcal{D}_{\text{val}}| \ll$
133 $|\mathcal{D}_{\text{train}}|$.

134 Suppose for every training sample z there exists t underlying hidden discrete attributes, $A' =$
135 $\{a^1, \dots, a^t\}$ and for each attribute (a^j) there are o possible values denoted as $V(a^j) \in \{b_1^j \dots b_o^j\}$.
136 In real-world settings, neural networks (θ^*) trained on $\mathcal{D}_{\text{train}}$ often associate class labels (y) with
137 specific attribute-value pairs (a^m, b_t^m) [43, 13, 14]. For example, a model trained to predict gender
138 might associate it with the feature "beard" (present/absent). However, feature imbalance in the datasets
139 can lead to misleading associations. If most of the male images in a dataset include smiles, the model
140 might spuriously link "male" with "smiling" rather than "beard." This can cause misclassification,

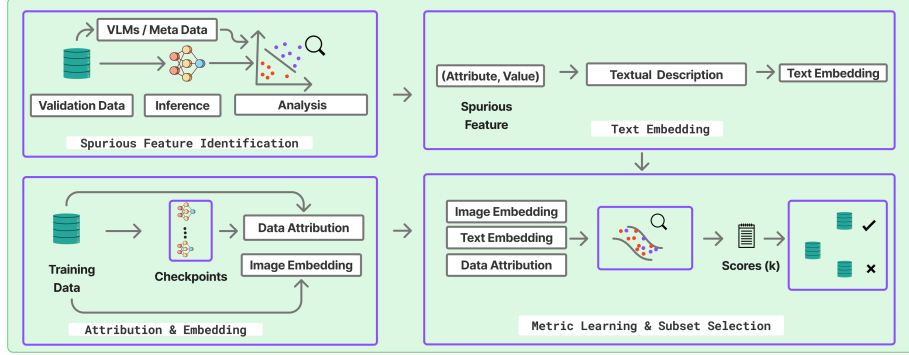


Figure 1: The figure illustrates the key steps in identifying detrimental samples. First, the performance of the model across different attribute value pairs is analyzed to identify and textually describe the underlying bias. Then, training samples that align with this bias and exhibit high detrimental attribution scores are selected for removal.

141 like predicting smiling females as males. We term such misleading attribute-value pairs as **spurious**
 142 **features**. In these scenarios, the primary objective of our work is to identify a set of detrimental
 143 examples, $\mathcal{S}^{\text{deter}} \in \mathcal{D}_{\text{train}}$, that “correspond” to the spurious features and might degrade the model’s
 144 performance. The model is then retrained from scratch on the filtered dataset, $(\mathcal{D}_{\text{train}} \setminus \mathcal{S}^{\text{deter}})$, to
 145 reduce the influence of the spurious feature in the training dataset similar to prior work like Chaudhuri
 146 et al. [28].

147 Our method for identifying $\mathcal{S}^{\text{deter}}$ involves two steps: (1) Annotate attribute–value pairs in the
 148 validation set to detect potential spurious features and generate a textual description of the bias; (2)
 149 Select $\mathcal{S}^{\text{deter}} \subset \mathcal{D}_{\text{train}}$ as samples semantically aligned with the bias and whose removal as per the
 150 data attribution scores does not degrade model performance.

151 3.2 Attribute Annotation and Spurious Feature Identification

152 A key component to identify spurious features is the availability of attribute–value annotations for the
 153 validation dataset. However, in many practical scenarios, such annotations are often missing from
 154 the metadata. Chen et al. [39] has shown that in the absence of such information, large language
 155 and vision models can be used to generate annotations necessary to identify the underlying spurious
 156 features. Hence, for datasets without pre-annotated attributes, we annotate the validation set with
 157 potential attribute–value pairs to assist in identifying spurious features.

158 To generate candidate attribute–value pairs, we leverage large language models such as ChatGPT [39].
 159 ChatGPT is provided with a simple task description and prompted to suggest relevant attributes and
 160 associated values. For example, for a gender classification task, it can generate attributes like “smile”,
 161 “beard”, with possible values as “presence” or “absence”. We adopt task-specific prompts proposed
 162 by Chen et al. [39] to guide this process. Once the attribute–value pairs are generated, the next step is
 163 to annotate the validation dataset. However, considering the limitations associated with ChatGPT
 164 for this task [39], we use Llama 3.2 [78], a vision–language model, to annotate the images in the
 165 validation dataset. Further details about the prompts can be found in Appendix G.

166 3.2.1 Spurious Feature Identification

167 To identify spurious features, we take motivation from recent work that tries to identify systematic
 168 bias in a model [42, 43] based on its accuracy and errors on the validation dataset. However, unlike
 169 previous methods, which try to identify underperforming subgroups that may require collecting
 170 additional data, we try to determine the overperforming attribute–value pair as a possible candidate
 171 for data deletion [79, 28]. For this, we take inspiration from Johnson et al. [42] and compare the
 172 performance of the dataset associated with each attribute–value pair to the performance of the entire
 173 dataset. If the performance gap exceeds a predefined threshold, the corresponding attribute–value pair
 174 is flagged as a potential spurious feature in the model. Formally, this is expressed as:

$$\frac{1}{|\mathcal{D}_\alpha|} \sum_{(x,y) \in \mathcal{D}_\alpha} \mathbf{1}(h(x) = y) - \frac{1}{|\mathcal{D}_{\text{val}}|} \sum_{(x,y) \in \mathcal{D}_{\text{val}}} \mathbf{1}(h(x) = y) > \tau, \quad (1)$$

175 where, \mathcal{D}_α is a subset of validation data \mathcal{D}_{val} associated with a^v attribute and it's j^{th} value b_j^v . The
 176 indicator function $\mathbf{1}$ indicates the correct prediction made by the model. The function $h(x)$ represents
 177 the prediction made by the model for a given input x , and y as the corresponding true class label. The
 178 parameter τ denotes the minimum threshold.

179 Once an attribute-value pair exceeds the threshold, a textual description is generated to describe
 180 the spurious feature. For example: "Images with $\{a\}$ as $\{b\}$." Here, (a, b) is the attribute value pair
 181 selected as per Equation 1. Details about the textual description are provided in Appendix H.4.

182 3.3 Coherent Data Attribution

183 After generating the desired text, the next task is to select a subset of data that is semantically coherent
 184 with the given text and whose removal can improve the performance of the model [80].

185 Since our task involves efficient subset selection, we formally define data attribution as follows:

186 **Definition 1** (Data Attribution and Leave-one-out Influence Score [32]). *Given training dataset*
 187 $\mathcal{D}_{\text{train}}$, *and a model's utility function* $\mathbf{f}(v; \theta)$ *that measures the performance of the model, the data*
 188 *attribution score* $\alpha : \mathcal{D}_{\text{train}} \times \mathcal{D}_{\text{val}} \rightarrow \mathcal{R}$ *is defined as the change in the model's prediction for a*
 189 *validation sample v_i with respect to the optimal parameters when the training example z_k is excluded*
 190 *from the training dataset during the learning of the optimal parameters θ^* . Formally,*

$$\alpha(v_i; z_k) = \mathbf{f}\left(v_i; \theta^*(\mathcal{D}_{\text{train}})\right) - \mathbf{f}\left(v_i; \theta^*(\mathcal{D}_{\text{train}} \setminus z_k)\right) \quad (2)$$

191 For a classification task, the utility function $\mathbf{f}(z; \theta)$ for a sample $z = (x, y)$, [32], is defined as:

$$\mathbf{f}(z; \theta) = \log\left(\frac{p(z; \theta)}{1 - p(z; \theta)}\right), \quad (3)$$

192 where $p(z; \theta)$ represents the probability assigned to the correct class by the softmax function of
 193 a neural network parameterized by θ . A high $\mathbf{f}(z; \theta)$ corresponds to a high likelihood for a given
 194 sample (z) .

195 The NTK-based methods like Trak, have a closed-form formulation for data attribution score (α)
 196 (Definition 1) expressed as:

$$\begin{aligned} \alpha(v_j, z_i) &= \frac{1}{N} \sum_{n=1}^N \left(\phi_n(v_j)^\top (\Phi_n^\top \Phi_n)^{-1} \phi_n(z_i) \right) \\ &\quad \times \frac{1}{N} \sum_{n=1}^N \left(1 - p_n^{z_i} \right) \end{aligned} \quad (4)$$

197 where, for N different checkpoints of model (θ^*), $\{p_n^{z_i}\}$ represents the probability assigned by n^{th}
 198 set of parameters to the correct class (y_i), for sample $z_i = (x_i, y_i)$. The terms $\phi_n(v_j)$ and $\phi_n(z_i)$
 199 denote the projected gradients of the validation sample v_j and the training sample z_i with respect
 200 to the n^{th} set of optimal parameters, and for the utility function $(\mathbf{f}(\cdot; \theta_n^*))$. Additionally, Φ_n is
 201 the projected gradient for the entire training dataset. Further details about Trak can be found in
 202 Appendix B.

203 To quantify the impact of removing a data sample z from the training dataset on the performance of
 204 the entire validation dataset, we define the metric $\mathcal{A}(z)$ as a detrimental attribution score associated
 205 with the validation dataset for sample z . This metric measures the change in the model's performance
 206 (\mathbf{f}) for the validation dataset when z is excluded from the training dataset.

$$\begin{aligned} \mathcal{A}(z_i) &= - \sum_{v_j \in \mathcal{D}_{\text{val}}} \alpha(v_j, z_i) \\ &= \sum_{v_j \in \mathcal{D}_{\text{val}}} \left(\mathbf{f}(v_j; \theta^*(\mathcal{D}_{\text{train}} \setminus z_i)) - \mathbf{f}(v_j; \theta^*(\mathcal{D}_{\text{train}})) \right) \end{aligned} \quad (5)$$

207 where $z_i \in \mathcal{D}_{\text{train}}$. Unlike the data attribution score defined in Definition 1, $\mathcal{A}(z_i)$ is the negative
 208 of the general definition and evaluates the contribution of each training sample to the likelihood of
 209 the entire validation dataset. A higher value of $\mathcal{A}(z_i)$ indicates that removing the training sample z_i
 210 and retraining the model with the updated dataset leads to an optimal parameter θ^* that improves
 211 the likelihood of the validation dataset (Equation 3). In other words, training examples that degrade
 212 overall validation performance are assigned higher $\mathcal{A}(z_i)$ values. Once $\mathcal{A}(z_i)$ is calculated, it is
 213 normalized and used for further steps.

214 While removing samples with high $\mathcal{A}(z)$ values can improve the model’s performance; however,
 215 its impact on the downstream model is often tied up with its capability to remove samples with
 216 spurious features. During training, spurious features present in the dataset can result in gradient
 217 starvation [81, 61], a phenomenon that can hamper the learning of predictive features. Under such
 218 scenarios, we theoretically show that the detrimental attribution score(\mathcal{A}) for a data sample containing
 219 a spurious feature (f_1) can be lower than that of a data sample with predictive features (f_2), even
 220 when both features are equally represented. Consequently, deletion strategies based solely on high
 221 attribution scores may inadvertently remove examples with predictive rather than spurious features
 222 (Proposition 1) and can fail to capture the impact of removing data associated with spurious features
 223 on the overall generalization.

224 **Proposition 1** (Under Valuation of Attribution Scores). *Consider a neural network in the neural
 225 tangent kernel (NTK) regime, trained using binary cross-entropy loss with two equally informative
 226 features, f_1 and f_2 . lets assume that due to learning dynamics f_1 becomes dominant and causes
 227 gradient starvation of f_2 as per Pezeshki et al. [61]. Then, for two training samples z_i and z_j with
 228 equal representation of dominating features f_1 and f_2 , respectively. The attribution score for z_i can
 229 be systematically undervalued relative to z_j . Formally:*

$$|\mathcal{A}(z_i)| < |\mathcal{A}(z_j)|$$

230 The proof of Proposition 1, along with further details on gradient starvation, is provided in Appendix F.
 231 Empirical evidence supporting this phenomenon is presented in Appendix J.

232 This limitation of attribution scores motivates the need for a targeted removal strategy that specifically
 233 identifies and eliminates training samples sharing similar spurious features and exhibiting high $\mathcal{A}(z)$
 234 scores. In many practical scenarios, the information about spurious features is missing in the data.
 235 Although annotating the entire training dataset using VLM-based models is possible, this approach is
 236 often excessively time-consuming and practically infeasible, particularly for large-scale datasets [40].
 237 To address this, we adopt a zero-shot approach [82] and leverage textual descriptions of bias and CLIP
 238 embeddings to select data samples that are semantically similar to the identified textual descriptions.
 239 Specifically, we convert the textual description (Section 3.2) of the potential spurious feature into
 240 an embedding $\mathcal{C}_{\text{text}}$. Similarly, we convert all images in the training dataset into their corresponding
 241 CLIP embeddings $\mathcal{C}_{\text{image}}^i$ for $i \in 1, \dots, |\mathcal{D}_{\text{train}}|$. Each training sample z_i is then assigned a score \mathbf{k}_i ,
 242 reflecting its semantic similarity to the identified bias as per the given equation :

$$\mathbf{k}_i = \exp \left(- \frac{(\mathcal{C}_{\text{text}} - \mathcal{C}_{\text{image}}^i) M (\mathcal{C}_{\text{text}} - \mathcal{C}_{\text{image}}^i)^{\top}}{2} \right),$$

where, $M = LL^{\top}$, $L \in \mathbb{R}^{D \times t}$, $t \ll D$ (6)

243 The text and image features, denoted as $\mathcal{C}_{\text{text}}$, $\mathcal{C}_{\text{image}}^i \in \mathbb{R}^{1 \times D}$ are represented as row vectors in a
 244 D-dimensional space. The matrix M is a positive semi-definite matrix, constructed as the outer
 245 product of a low-rank matrix L (rank at most t), and can serve as a learnable transformation. Since M
 246 defines the distance metric, varying the values of L allows us to generate different similarity measures
 247 for comparing data points [37, 38].

248 We aim to remove data samples that have high \mathcal{A} scores and are semantically aligned with the
 249 identified bias. To achieve this, we learn the matrix L [83, 37, 38] by maximizing the weighted
 250 \mathcal{A} score for each sample, where higher weights indicate stronger semantic alignment with bias as
 251 per Equation 6. To maintain semantic coherence with the bias description, the cumulative score for
 252 the dataset is enforced to exceed a threshold \mathcal{T} , defined as a fraction (β) of the total training size
 253 ($|\mathcal{D}_{\text{train}}|$). A larger \mathcal{T} emphasizes semantic alignment, while a smaller \mathcal{T} allows for flexibility in

254 sample selection based on \mathcal{A} scores. The complete optimization objective is described as below :

$$\begin{aligned} \max_L \sum_{i=1}^{|\mathcal{D}_{\text{train}}|} \left(\frac{k_i}{\sum_j k_j} \right) \mathcal{A}(z_i) \\ \text{s.t. } \sum_{i=1}^{|\mathcal{D}_{\text{train}}|} k_i \geq \mathcal{T}, \quad \mathcal{T} = \beta \times |\mathcal{D}_{\text{train}}|. \end{aligned} \quad (7)$$

255 To ensure that the optimization remains tractable, we replace the hard constraint with a soft penalty
256 term [83] in the objective function. Further detail on this is provided in Appendix C.

257 Once the optimization is complete, a subset of training data with k_i scores greater than the hyper-
258 parameter γ is selected for removal ($\mathcal{S}^{\text{deter}}$). The model is then retrained with the updated training
259 dataset ($\mathcal{D}_{\text{train}} \setminus \mathcal{S}^{\text{deter}}$) where, $\mathcal{S}^{\text{deter}} = \{z_i \in \mathcal{D}_{\text{train}} \mid k_i > \gamma\}$. A sensitivity analysis of all the
260 hyperparameters, and comparison with only CLIP and only data attribution on overall performance is
261 provided in Appendix Q and Appendix M, respectively.

262 4 Experiments

263 4.1 Setting

264 We evaluate the performance of our method across various datasets and compare it with existing data
265 attribution techniques, including original training of model with complete dataset (original), Random
266 deletion of data points (Random), Influence Function (IF) [30], TracIN [58], EWC Repair [31], and
267 Trak [32]. The datasets used in our experiments include WaterBirds [84], Animal with attributes
268 (AWA2) [85], German Traffic Sign Recognition Benchmark (GTSRB) [86], CELEBA [87, 43, 88]
269 (Appendix H), CIFAR-10 [89], and ImageNet-100 [90, 91]. Further comparisons with robustness-
270 based methods(groupDRO [17], JTT [16]) and group balancing methods are provided in Appendix I.
271 For datasets such as GTSRB, CIFAR-10, and WaterBirds, we utilized attributes generated by ChatGPT
272 and VLM models. To further assess the impact of metadata availability, we created two variants
273 for the AWA2 datasets. The first variant, AWA2-A, includes class-specific annotations provided by
274 the original datasets. The second variant, AWA2-B, uses attributes generated using ChatGPT and
275 VLM-based annotation techniques (Section 3.2). All Primary experiments were conducted using a
276 ResNet-18 model, which is the base architecture used in NTK-based data attribution methods such as
277 Trak [32] for the image classification task. Additional experiments using alternative architectures
278 and vision transformer models are presented in Appendix N and Appendix O, respectively. We
279 have reported the worst group accuracy and average accuracy based on prior work on spurious
280 features [67, 17, 28]. However, due to the absence of well-defined group structures in many real-
281 world datasets [17], we have compared these datasets on average accuracy and class-level accuracy.
282 All the experiments were conducted on two NVIDIA A6000 GPUs. Further details on training,
283 hyperparameters, and subset size are provided in Appendix H. Algorithm 1 (Appendix) illustrates the
284 overall workflow of our approach. We also report time and memory overheads associated with subset
285 selection in Appendix R and Appendix S, respectively. Sample images from the selected subset $\mathcal{S}^{\text{deter}}$
286 are shown in Appendix U.

287 4.2 Improvement in Average Accuracy

288 Table 1 reports the improvement in average accuracy achieved by our method compared to existing
289 baselines. On average, our method outperforms Trak by 1.4%, EWC by 1.6%, TracIN by 1.4%,
290 Influence Functions by 2.0%, and the original full-dataset training baseline by 1.7%. Notably,
291 we observe gains of 1.9%, 2.5%, and 2.4% over Trak on AWA2-B, WaterBirds, and AWA2-A,
292 respectively. The performance improvement highlights the efficiency of our method in removing the
293 detrimental samples associated with spurious features. We further saw a substantial improvement in
294 under represented class as discussed in Section 4.3. Additional experiments on worst-group accuracy
295 and architectural ablations for WaterBirds are provided in Appendix N.

296 4.3 Class Level Improvement after Data Deletion

297 Table 2 presents class-level accuracy for datasets with more than two classes. As per the results, our
298 method improves the accuracy of a significant number of classes across datasets. For example, in

Table 1: Comparative evaluation of average accuracy of our proposed method (Ours) against baseline approaches across multiple datasets. The results report mean accuracy scores over three independent runs, with the best-performing values highlighted in **bold**. Entries with a gain of more than **1.5%** over full-data training are highlighted in orange, while those exceeding **3%** are shown in blue.

Dataset	Original	Random	IF	TracIN	EWC	Trak	Ours
WaterBirds	0.638	0.606	0.603	0.652	0.650	0.656	0.681
AWA2-A	0.644	0.622	0.644	0.652	0.642	0.638	0.662
CELEBA	0.895	0.893	0.890	0.893	0.890	0.898	0.906
GTSRB	0.969	0.966	0.973	0.971	0.975	0.971	0.980
AWA2-B	0.644	0.622	0.644	0.652	0.642	0.638	0.657
CIFAR-10	0.774	0.787	0.798	0.784	0.789	0.793	0.801
ImageNet-100	0.440	0.436	0.429	0.423	0.423	0.435	0.438

Table 2: Class-level accuracy improvement(Imp) after data removal across datasets. The table shows the maximum improvement in any class, the number of improved classes, and the mean improvement across them.

Dataset	Max Imp	# Imp Classes	Mean Imp
Awa2-A	16.27%	6 / 10	11.12%
Awa2-B	29.16%	4 / 10	17.98%
CIFAR-10	10.39%	7 / 10	5.59%
GTSRB	50.00%	22 / 43	5.69%
ImageNet-100	36.00 %	51 / 100	10.15%

299 Awa2-A, Awa2-B, ImageNet-100, and CIFAR-10, over 40% of the classes show improvement, with
300 some achieving gains as high as 29.16%. Notably, in GTSRB, 22 out of 43 classes benefit, with a
301 maximum per-class improvement of 50%. The improvement in average accuracy highlights that the
302 improvement in underperforming classes is attained without substantially degrading the performance
of other classes. Details on worst-class accuracy are provided in Appendix K.

Table 3: Comparison of best average accuracy across different data attribution methods for different spurious attributes. The table reports the mean accuracy across three independent runs. Entries with a gain of more than **1.5%** over full-data training are highlighted in orange, while those exceeding **3%** are shown in blue.

Target	Spurious Attribute	Original	Maj.-Rand	Random	IF	EWC	TracIN	Trak	Ours
arched eyebrows	receding hairline	0.713	0.740	0.739	0.716	0.724	0.730	0.722	0.736
attractive	mouth slightly open	0.628	0.627	0.668	0.640	0.633	0.631	0.658	0.673
big nose	male	0.771	0.770	0.770	0.764	0.751	0.745	0.756	0.780
goatee	bushy eyebrows	0.946	0.931	0.947	0.938	0.951	0.953	0.949	0.953
mouth slightly open	smiling	0.869	0.871	0.877	0.877	0.860	0.876	0.867	0.877
mouth slightly open	wearing lipstick	0.820	0.804	0.801	0.828	0.834	0.816	0.801	0.839
narrow eyes	eyeglasses	0.840	0.858	0.862	0.856	0.858	0.860	0.855	0.862
pointy nose	mouth slightly open	0.690	0.714	0.676	0.689	0.695	0.709	0.694	0.698
receding hairline	rosy cheeks	0.921	0.909	0.920	0.921	0.920	0.916	0.911	0.930
male	pointy nose	0.919	0.931	0.907	0.909	0.911	0.906	0.915	0.921

303

304 4.4 Performance across Different Spurious Attributes

305 To further investigate the impact of spurious features on both worst-group and average performance,
306 we follow the setup of Eyuboglu et al. [43] and select a subset of the CELEBA dataset where the target
307 attribute is strongly correlated with a spurious feature. We compare the average and worst-group
308 performance achieved by our method against other baselines in Table 3 and Table 4. Additionally,
309 considering the benefit of random data deletion in biased dataset [28] we introduce a new baseline,
310 Maj.-Rand, where the subset of data is randomly deleted from the majority group. As shown in the
311 results, our method outperforms other baselines in average accuracy in 7 and worst-group accuracy
312 in 8 out of 10 settings, respectively. Notably, we observe a gain of over 4% in average accuracy for
313 the target attribute attractive, compared to training on the original dataset. Similarly, worst-group
314 accuracy improves by over 15% for attractive, receding hairline, and arched eyebrows, and by more
315 than 5% for big nose, goatee, and male.

Table 4: Comparison of best worst-group accuracy across different data attribution methods for different spurious attributes. The table reports the mean accuracy across three independent runs. Entries with a gain of more than 5% over full-data training are highlighted in green, while those exceeding 15% are shown in violet.

Target	Spurious Attribute	Original	Maj.-Rand	Random	IF	EWC	TracIN	Trak	Ours
arched eyebrows	receding hairline	0.187	0.314	0.113	0.247	0.262	0.196	0.099	0.354
attractive	mouth slightly open	0.213	0.242	0.347	0.266	0.241	0.205	0.392	0.407
big nose	male	0.131	0.076	0.096	0.143	0.092	0.113	0.172	0.221
goatee	bushy eyebrows	0.432	0.493	0.287	0.437	0.439	0.387	0.278	0.548
mouth slightly open	smiling	0.524	0.415	0.552	0.418	0.441	0.487	0.433	0.489
mouth slightly open	wearing lipstick	0.555	0.471	0.557	0.598	0.594	0.549	0.486	0.612
narrow eyes	eyeglasses	0.208	0.052	0.119	0.000	0.092	0.128	0.024	0.151
pointy nose	mouth slightly open	0.045	0.044	0.046	0.034	0.028	0.021	0.040	0.084
receding hairline	rosy cheeks	0.121	0.228	0.131	0.179	0.241	0.254	0.201	0.296
male	pointy nose	0.840	0.882	0.824	0.833	0.861	0.870	0.875	0.903

Table 5: Comparison of best average and best worst-group accuracy between metadata-driven and VLM-guided textual description.

Target	Sp. Attribute	Meta Data		VLM	
		Avg. Acc.	WG Acc.	Avg. Acc.	WG Acc.
bangs	black hair	0.922	0.649	0.916	0.624
big nose	wearing necklace	0.787	0.347	0.776	0.236
heavy makeup	straight hair	0.826	0.716	0.835	0.716
wearing earrings	bags under eyes	0.798	0.281	0.791	0.214

Table 6: Comparison of best average and best worst-group accuracy between our method and D3M across different spurious attributes.

Target	Spurious Attribute	Ours		D3M	
		Avg. Acc.	WG Acc.	Avg. Acc.	WG Acc.
bangs	black hair	0.922	0.649	0.920	0.627
big nose	wearing necklace	0.787	0.347	0.747	0.173
heavy makeup	straight hair	0.826	0.716	0.821	0.654
wearing earrings	bags under eyes	0.798	0.281	0.787	0.068

316 4.5 Ablation between Meta Data and VLM-based Description

317 Table 5 compares the performance of our method when using metadata versus VLM-generated textual
318 descriptions of the spurious feature. While both strategies show comparable performance in terms
319 of average accuracy, the metadata-driven variant generally achieves higher worst-group accuracy.
320 This shows that a better annotation of underlying bias can help in the targeted removal of detrimental
321 samples. However, even in the absence of such annotation, LLM and VLM-based methods can
322 generate comparative performance.

323 4.6 Comparison with Group Annotation based Subset Selection

324 Table 6 presents a comparative evaluation between our method, which relies on the textual description
325 of bias, against a technique that can use group annotation of spurious features in the validation
326 dataset. To compare with such a method, we define group structure based on different values of
327 Spurious Attribute and Target, and then use the method proposed by Jain et al. [11] (D3M) for subset
328 selection. As per the result, on average, our method consistently outperforms D3M across both the
329 best average and worst-group accuracy with a gain of 1.5% in best average accuracy and 11.8% in
330 best worst group accuracy without using the explicit group annotation. This highlights the efficiency
331 of the soft comparison scheme of clip features in handling partially visible features and the proposed
332 optimization scheme compared to hard thresholding used in group annotation.

333 5 Conclusion

334 In this work, we propose a data deletion framework to mitigate the impact of spurious biases in the
335 training dataset and enhance model performance. Our method employs metric learning techniques
336 to target and remove training samples that are semantically aligned with the textual description of
337 identified biases and whose removal, based on attribution scores, does not adversely affect model
338 performance. To the best of our knowledge, this is the first approach to use text-guided data attribution
339 scores to mitigate simplicity bias in models. However, its effectiveness depends on the quality of the
340 textual descriptions used to capture spurious biases, and the current framework is limited to image
341 datasets. In future work, we aim to incorporate a human-in-the-loop framework to better mitigate
342 complex biases and to extend it to NLP tasks.

343 **References**

344 [1] Nikita Bhatt, Nirav Bhatt, Purvi Prajapati, Vishal Sorathiya, Samah Alshathri, and Walid El-Shafai. A
345 data-centric approach to improve performance of deep learning models. *Scientific Reports*, 14(1):22329, 2024.

347 [2] Steven Euijong Whang, Yuji Roh, Hwanjun Song, and Jae-Gil Lee. Data collection and quality challenges
348 in deep learning: A data-centric ai perspective. *The VLDB Journal*, 32(4):791–813, 2023.

349 [3] Xinyi Xu, Shuaiqi Wang, Chuan-Sheng Foo, Bryan Kian Hsiang Low, and Giulia Fanti. Data distribution
350 valuation. *arXiv preprint arXiv:2410.04386*, 2024.

351 [4] Sang Keun Choe, Hwijeon Ahn, Juhan Bae, Kewen Zhao, Minsoo Kang, Youngseog Chung, Adithya
352 Pratapa, Willie Neiswanger, Emma Strubell, Teruko Mitamura, et al. What is your data worth to gpt?
353 llm-scale data valuation with influence functions. *arXiv preprint arXiv:2405.13954*, 2024.

354 [5] Zhipeng Xu, Zhenghao Liu, Yukun Yan, Zhiyuan Liu, Ge Yu, and Chenyan Xiong. Cleaner pretraining
355 corpus curation with neural web scraping. *arXiv preprint arXiv:2402.14652*, 2024.

356 [6] Jay M Patel and Jay M Patel. Introduction to common crawl datasets. *Getting structured data from the*
357 *internet: running web crawlers/scrapers on a big data production scale*, pages 277–324, 2020.

358 [7] Rodrigo F Berriel, Franco Schmidt Rossi, Alberto F de Souza, and Thiago Oliveira-Santos. Automatic
359 large-scale data acquisition via crowdsourcing for crosswalk classification: A deep learning approach.
360 *Computers & graphics*, 68:32–42, 2017.

361 [8] Alexey Drutsa, Viktoriya Farafonova, Valentina Fedorova, Olga Megorskaya, Evfrosiniya Zerminova, and
362 Olga Zhilinskaya. Practice of efficient data collection via crowdsourcing at large-scale. *arXiv preprint*
363 *arXiv:1912.04444*, 2019.

364 [9] David Thiel. Identifying and eliminating csam in generative ml training data and models. *Stanford*
365 *Internet Observatory, Cyber Policy Center, December*, 23:3, 2023.

366 [10] Emilio Ferrara. Fairness and bias in artificial intelligence: A brief survey of sources, impacts, and
367 mitigation strategies. *Sci*, 6(1):3, 2023.

368 [11] Saachi Jain, Kimia Hamidieh, Kristian Georgiev, Andrew Ilyas, Marzyeh Ghassemi, and Aleksander
369 Madry. Improving subgroup robustness via data selection. *Advances in Neural Information Processing*
370 *Systems*, 37:94490–94511, 2024.

371 [12] Pang Wei Koh, Shiori Sagawa, Henrik Marklund, Sang Michael Xie, Marvin Zhang, Akshay Balsubramani,
372 Weihua Hu, Michihiro Yasunaga, Richard Lanas Phillips, Irena Gao, et al. Wilds: A benchmark of
373 in-the-wild distribution shifts. In *International conference on machine learning*, pages 5637–5664. PMLR,
374 2021.

375 [13] Rishabh Tiwari and Pradeep Shenoy. Overcoming simplicity bias in deep networks using a feature sieve.
376 In *International Conference on Machine Learning*, pages 34330–34343. PMLR, 2023.

377 [14] Robert Geirhos, Jörn-Henrik Jacobsen, Claudio Michaelis, Richard Zemel, Wieland Brendel, Matthias
378 Bethge, and Felix A Wichmann. Shortcut learning in deep neural networks. *Nature Machine Intelligence*,
379 2(11):665–673, 2020.

380 [15] RT McCoy. Right for the wrong reasons: Diagnosing syntactic heuristics in natural language inference.
381 *arXiv preprint arXiv:1902.01007*, 2019.

382 [16] Evan Z Liu, Behzad Haghgoo, Annie S Chen, Aditi Raghunathan, Pang Wei Koh, Shiori Sagawa, Percy
383 Liang, and Chelsea Finn. Just train twice: Improving group robustness without training group information.
384 In *International Conference on Machine Learning*, pages 6781–6792. PMLR, 2021.

385 [17] Shiori Sagawa, Pang Wei Koh, Tatsunori B Hashimoto, and Percy Liang. Distributionally robust neural
386 networks for group shifts: On the importance of regularization for worst-case generalization. *arXiv*
387 *preprint arXiv:1911.08731*, 2019.

388 [18] Jungsoo Lee, Eungyeup Kim, Juyoung Lee, Jihyeon Lee, and Jaegul Choo. Learning debiased represen-
389 tation via disentangled feature augmentation. *Advances in Neural Information Processing Systems*, 34:
390 25123–25133, 2021.

391 [19] Sheng Liu, Xu Zhang, Nitesh Sekhar, Yue Wu, Prateek Singhal, and Carlos Fernandez-Granda. Avoiding
392 spurious correlations via logit correction. *arXiv preprint arXiv:2212.01433*, 2022.

393 [20] Tyler LaBonte, Vidya Muthukumar, and Abhishek Kumar. Towards last-layer retraining for group
 394 robustness with fewer annotations. *Advances in Neural Information Processing Systems*, 36:11552–11579,
 395 2023.

396 [21] Gavin S Hartnett, Andrew J Lohn, and Alexander P Sedlack. Adversarial examples for cost-sensitive
 397 classifiers. *arXiv preprint arXiv:1910.02095*, 2019.

398 [22] Kunyang Li, Jean-Charles Noirot Ferrand, Ryan Sheetsley, Blaine Hoak, Yohan Beugin, Eric Pauley, and
 399 Patrick McDaniel. On the robustness tradeoff in fine-tuning. *arXiv preprint arXiv:2503.14836*, 2025.

400 [23] Pavan Kalyan Reddy Neerudu, Subba Reddy Oota, Mounika Marreddy, Venkateswara Rao Kagita,
 401 and Manish Gupta. On robustness of finetuned transformer-based nlp models. *arXiv preprint
 402 arXiv:2305.14453*, 2023.

403 [24] Chester Holtz, Tsui-Wei Weng, and Gal Mishne. Learning sample reweighting for accuracy and adversarial
 404 robustness. *arXiv preprint arXiv:2210.11513*, 2022.

405 [25] Shiqi Wang, Kexin Pei, Justin Whitehouse, Junfeng Yang, and Suman Jana. Efficient formal safety
 406 analysis of neural networks. *Advances in neural information processing systems*, 31, 2018.

407 [26] Eric Wong and Zico Kolter. Provable defenses against adversarial examples via the convex outer
 408 adversarial polytope. In *International conference on machine learning*, pages 5286–5295. PMLR, 2018.

409 [27] Feng Xiong, Maoyue Xie, Lingjuan Zhao, Cheng Li, and Xuan Fan. Recognition and evaluation of data
 410 as intangible assets. *Sage Open*, 12(2):21582440221094600, 2022.

411 [28] Kamalika Chaudhuri, Kartik Ahuja, Martin Arjovsky, and David Lopez-Paz. Why does throwing away
 412 data improve worst-group error? In *International Conference on Machine Learning*, pages 4144–4188.
 413 PMLR, 2023.

414 [29] Badr Youbi Idrissi, Martin Arjovsky, Mohammad Pezeshki, and David Lopez-Paz. Simple data balancing
 415 achieves competitive worst-group-accuracy. In *Conference on Causal Learning and Reasoning*, pages
 416 336–351. PMLR, 2022.

417 [30] Pang Wei Koh and Percy Liang. Understanding black-box predictions via influence functions. In
 418 *International conference on machine learning*, pages 1885–1894. PMLR, 2017.

419 [31] Ryutaro Tanno, Melanie F Pradier, Aditya Nori, and Yingzhen Li. Repairing neural networks by leaving
 420 the right past behind. *Advances in Neural Information Processing Systems*, 35:13132–13145, 2022.

421 [32] Sung Min Park, Kristian Georgiev, Andrew Ilyas, Guillaume Leclerc, and Aleksander Madry. Trak:
 422 Attributing model behavior at scale. *arXiv preprint arXiv:2303.14186*, 2023.

423 [33] Logan Engstrom, Axel Feldmann, and Aleksander Madry. Dsdm: Model-aware dataset selection with
 424 datamodels. *arXiv preprint arXiv:2401.12926*, 2024.

425 [34] Mengzhou Xia, Sadhika Malladi, Suchin Gururangan, Sanjeev Arora, and Danqi Chen. Less: Selecting
 426 influential data for targeted instruction tuning. *arXiv preprint arXiv:2402.04333*, 2024.

427 [35] Max Marion, Ahmet Üstün, Luiza Pozzobon, Alex Wang, Marzieh Fadaee, and Sara Hooker. When less
 428 is more: Investigating data pruning for pretraining llms at scale. *arXiv preprint arXiv:2309.04564*, 2023.

429 [36] Alec Radford, Jong Wook Kim, Chris Hallacy, Aditya Ramesh, Gabriel Goh, Sandhini Agarwal, Girish
 430 Sastry, Amanda Askell, Pamela Mishkin, Jack Clark, et al. Learning transferable visual models from
 431 natural language supervision. In *International conference on machine learning*, pages 8748–8763. PMLR,
 432 2021.

433 [37] Daryl Lim and Gert Lanckriet. Efficient learning of mahalanobis metrics for ranking. In *International
 434 conference on machine learning*, pages 1980–1988. PMLR, 2014.

435 [38] Usha Bhalla, Alex Oesterling, Suraj Srinivas, Flavio P Calmon, and Himabindu Lakkaraju. Interpreting
 436 clip with sparse linear concept embeddings (splice). *arXiv preprint arXiv:2402.10376*, 2024.

437 [39] Muxi Chen, Yu Li, and Qiang Xu. Hibug: on human-interpretable model debug. *Advances in Neural
 438 Information Processing Systems*, 36, 2024.

439 [40] Haoming Lu and Feifei Zhong. Can vision-language models replace human annotators: A case study
 440 with celeba dataset. *arXiv preprint arXiv:2410.09416*, 2024.

441 [41] Zhen Tan, Dawei Li, Song Wang, Alimohammad Beigi, Bohan Jiang, Amrita Bhattacharjee, Mansooreh
 442 Karami, Jundong Li, Lu Cheng, and Huan Liu. Large language models for data annotation and synthesis:
 443 A survey. In *Proceedings of the 2024 Conference on Empirical Methods in Natural Language Processing*,
 444 pages 930–957, 2024.

445 [42] Nari Johnson, Ángel Alexander Cabrera, Gregory Plumb, and Ameet Talwalkar. Where does my model
 446 underperform? a human evaluation of slice discovery algorithms. In *Proceedings of the AAAI Conference*
 447 on *Human Computation and Crowdsourcing*, volume 11, pages 65–76, 2023.

448 [43] Sabri Eyuboglu, Maya Varma, Khaled Saab, Jean-Benoit Delbrouck, Christopher Lee-Messer, Jared
 449 Dunnmon, James Zou, and Christopher Ré. Domino: Discovering systematic errors with cross-modal
 450 embeddings. *arXiv preprint arXiv:2203.14960*, 2022.

451 [44] Chih-Kuan Yeh, Joon Kim, Ian En-Hsu Yen, and Pradeep K Ravikumar. Representer point selection for
 452 explaining deep neural networks. *Advances in neural information processing systems*, 31, 2018.

453 [45] Siyi Tang, Amirata Ghorbani, Rikiya Yamashita, Sameer Rehman, Jared A Dunnmon, James Zou, and
 454 Daniel L Rubin. Data valuation for medical imaging using shapley value and application to a large-scale
 455 chest x-ray dataset. *Scientific reports*, 11(1):8366, 2021.

456 [46] Harshay Shah, Sung Min Park, Andrew Ilyas, and Aleksander Madry. Modeldiff: A framework for
 457 comparing learning algorithms. In *International Conference on Machine Learning*, pages 30646–30688.
 458 PMLR, 2023.

459 [47] Roger Grosse, Juhan Bae, Cem Anil, Nelson Elhage, Alex Tamkin, Amirhossein Tajdini, Benoit Steiner,
 460 Dustin Li, Esin Durmus, Ethan Perez, et al. Studying large language model generalization with influence
 461 functions. *arXiv preprint arXiv:2308.03296*, 2023.

462 [48] Anshuman Chhabra, Peizhao Li, Prasant Mohapatra, and Hongfu Liu. " what data benefits my classifier?"
 463 enhancing model performance and interpretability through influence-based data selection. In *The Twelfth*
 464 *International Conference on Learning Representations*, 2024.

465 [49] Chenwang Wu, Defu Lian, Yong Ge, Zhihao Zhu, and Enhong Chen. Influence-driven data poisoning for
 466 robust recommender systems. *IEEE Transactions on Pattern Analysis and Machine Intelligence*, 45(10):
 467 11915–11931, 2023.

468 [50] Frank R Hampel. The influence curve and its role in robust estimation. *Journal of the american statistical*
 469 *association*, 69(346):383–393, 1974.

470 [51] Daryl Pregibon. Logistic regression diagnostics. *The annals of statistics*, 9(4):705–724, 1981.

471 [52] Rupert G Miller. The jackknife-a review. *Biometrika*, 61(1):1–15, 1974.

472 [53] Kamiar Rahnama Rad and Arian Maleki. A scalable estimate of the extra-sample prediction error via
 473 approximate leave-one-out. *arXiv preprint arXiv:1801.10243*, 2018.

474 [54] Ryan Giordano, William Stephenson, Runjing Liu, Michael Jordan, and Tamara Broderick. A swiss army
 475 infinitesimal jackknife. In *The 22nd International Conference on Artificial Intelligence and Statistics*,
 476 pages 1139–1147. PMLR, 2019.

477 [55] Juhan Bae, Nathan Ng, Alston Lo, Marzyeh Ghassemi, and Roger B Grosse. If influence functions are the
 478 answer, then what is the question? *Advances in Neural Information Processing Systems*, 35:17953–17967,
 479 2022.

480 [56] Samyadeep Basu, Philip Pope, and Soheil Feizi. Influence functions in deep learning are fragile. *arXiv*
 481 *preprint arXiv:2006.14651*, 2020.

482 [57] Zayd Hammoudeh and Daniel Lowd. Identifying a training-set attack's target using renormalized influence
 483 estimation. In *Proceedings of the 2022 ACM SIGSAC Conference on Computer and Communications*
 484 Security, pages 1367–1381, 2022.

485 [58] Garima Pruthi, Frederick Liu, Satyen Kale, and Mukund Sundararajan. Estimating training data influence
 486 by tracing gradient descent. *Advances in Neural Information Processing Systems*, 33:19920–19930, 2020.

487 [59] Andrew Ilyas, Sung Min Park, Logan Engstrom, Guillaume Leclerc, and Aleksander Madry. Datamodels:
 488 Predicting predictions from training data. *arXiv preprint arXiv:2202.00622*, 2022.

489 [60] Wenqian Ye, Guangtao Zheng, Xu Cao, Yunsheng Ma, and Aidong Zhang. Spurious correlations in
 490 machine learning: A survey. *arXiv preprint arXiv:2402.12715*, 2024.

491 [61] Mohammad Pezeshki, Oumar Kaba, Yoshua Bengio, Aaron C Courville, Doina Precup, and Guillaume
 492 Lajoie. Gradient starvation: A learning proclivity in neural networks. *Advances in Neural Information
 493 Processing Systems*, 34:1256–1272, 2021.

494 [62] Megha Srivastava, Tatsunori Hashimoto, and Percy Liang. Robustness to spurious correlations via human
 495 annotations. In *International Conference on Machine Learning*, pages 9109–9119. PMLR, 2020.

496 [63] Aahlad Puli, Nitish Joshi, Yoav Wald, He He, and Rajesh Ranganath. Nuisances via negativa: Adjusting
 497 for spurious correlations via data augmentation. *arXiv preprint arXiv:2210.01302*, 2022.

498 [64] Huaxiu Yao, Yu Wang, Sai Li, Linjun Zhang, Weixin Liang, James Zou, and Chelsea Finn. Improving
 499 out-of-distribution robustness via selective augmentation. In *International Conference on Machine
 500 Learning*, pages 25407–25437. PMLR, 2022.

501 [65] Xiangji Zeng, Yunliang Li, Yuchen Zhai, and Yin Zhang. Counterfactual generator: A weakly-supervised
 502 method for named entity recognition. In *Proceedings of the 2020 Conference on Empirical Methods in
 503 Natural Language Processing (EMNLP)*, pages 7270–7280, 2020.

504 [66] Shirley Wu, Mert Yuksekgonul, Linjun Zhang, and James Zou. Discover and cure: Concept-aware
 505 mitigation of spurious correlation. In *International Conference on Machine Learning*, pages 37765–
 506 37786. PMLR, 2023.

507 [67] Junhyun Nam, Jaehyung Kim, Jaeho Lee, and Jinwoo Shin. Spread spurious attribute: Improving
 508 worst-group accuracy with spurious attribute estimation. *arXiv preprint arXiv:2204.02070*, 2022.

509 [68] Tan Wang, Chang Zhou, Qianru Sun, and Hanwang Zhang. Causal attention for unbiased visual
 510 recognition. In *Proceedings of the IEEE/CVF International Conference on Computer Vision*, pages
 511 3091–3100, 2021.

512 [69] Daniel Levy, Yair Carmon, John C Duchi, and Aaron Sidford. Large-scale methods for distributionally
 513 robust optimization. *Advances in Neural Information Processing Systems*, 33:8847–8860, 2020.

514 [70] Polina Kirichenko, Pavel Izmailov, and Andrew Gordon Wilson. Last layer re-training is sufficient for
 515 robustness to spurious correlations. *arXiv preprint arXiv:2204.02937*, 2022.

516 [71] Eike Petersen, Yannik Potdevin, Esfandiar Mohammadi, Stephan Zidowitz, Sabrina Breyer, Dirk Nowotka,
 517 Sandra Henn, Ludwig Pechmann, Martin Leucker, Philipp Rostalski, et al. Responsible and regulatory
 518 conform machine learning for medicine: a survey of challenges and solutions. *IEEE Access*, 10:58375–
 519 58418, 2022.

520 [72] Michael Matheny, S Thadaney Israni, Mahnoor Ahmed, and Danielle Whicher. Artificial intelligence in
 521 health care: The hope, the hype, the promise, the peril. *Washington, DC: National Academy of Medicine*,
 522 10, 2019.

523 [73] Xudong Shen, Hannah Brown, Jiashu Tao, Martin Strobel, Yao Tong, Akshay Narayan, Harold Soh, and
 524 Finale Doshi-Velez. Towards regulatable ai systems: Technical gaps and policy opportunities. *arXiv
 525 preprint arXiv:2306.12609*, 2023.

526 [74] Francisco Javier Campos Zabala. Responsible ai understanding the ethical and regulatory implications of
 527 ai. In *Grow Your Business with AI: A First Principles Approach for Scaling Artificial Intelligence in the
 528 Enterprise*, pages 453–477. Springer, 2023.

529 [75] Romeo Valentin. Towards a framework for deep learning certification in safety-critical applications using
 530 inherently safe design and run-time error detection. *arXiv preprint arXiv:2403.14678*, 2024.

531 [76] Ziquan Liu, Zhuo Zhi, Ilija Bogunovic, Carsten Gerner-Beuerle, and Miguel Rodrigues. Prosac: Provably
 532 safe certification for machine learning models under adversarial attacks. *arXiv preprint arXiv:2402.02629*,
 533 2024.

534 [77] Timothée Lesort. Spurious features in continual learning. In *AAAI Bridge Program on Continual
 535 Causality*, pages 59–62. PMLR, 2023.

536 [78] Abhimanyu Dubey, Abhinav Jauhri, Abhinav Pandey, Abhishek Kadian, Ahmad Al-Dahle, Aiesha
 537 Letman, Akhil Mathur, Alan Schelten, Amy Yang, Angela Fan, et al. The llama 3 herd of models. *arXiv
 538 preprint arXiv:2407.21783*, 2024.

539 [79] Ming-Chang Chiu, Pin-Yu Chen, and Xuezhe Ma. Better may not be fairer: A study on subgroup
 540 discrepancy in image classification. In *Proceedings of the IEEE/CVF International Conference on
 541 Computer Vision*, pages 4956–4966, 2023.

542 [80] Long-Kai Huang, Peilin Zhao, Junzhou Huang, and Sinno Pan. Retaining beneficial information from
543 detrimental data for neural network repair. *Advances in Neural Information Processing Systems*, 36, 2024.

544 [81] Remi Tachet, Mohammad Pezeshki, Saeid Shabanian, Aaron Courville, and Yoshua Bengio. On the
545 learning dynamics of deep neural networks. *arXiv preprint arXiv:1809.06848*, 2018. URL <https://arxiv.org/abs/1809.06848>.

547 [82] Fei Pan, Sangryul Jeon, Brian Wang, Frank Mckenna, and Stella X Yu. Zero-shot building attribute
548 extraction from large-scale vision and language models. In *Proceedings of the IEEE/CVF Winter*
549 *Conference on Applications of Computer Vision*, pages 8647–8656, 2024.

550 [83] Gabriel d’Eon, Jonathan d’Eon, James R. Wright, and Kevin Leyton-Brown. The spotlight: A general
551 method for discovering systematic errors in deep learning models. In *Proceedings of the 2022 ACM*
552 *Conference on Fairness, Accountability, and Transparency*, pages 1962–1981, New York, NY, USA, June
553 2022. ACM. doi: 10.1145/3531146.3534641.

554 [84] Shiori Sagawa*, Pang Wei Koh*, Tatsunori B. Hashimoto, and Percy Liang. Distributionally robust neural
555 networks. In *International Conference on Learning Representations*, 2020. URL <https://openreview.net/forum?id=ryxGuJrFvS>.

557 [85] Yongqin Xian, Christoph H Lampert, Bernt Schiele, and Zeynep Akata. Zero-shot learning—a compre-
558 hensive evaluation of the good, the bad and the ugly. *IEEE transactions on pattern analysis and machine*
559 *intelligence*, 41(9):2251–2265, 2018.

560 [86] J. Stallkamp, M. Schlipsing, J. Salmen, and C. Igel. Man vs. computer: Benchmarking machine learning
561 algorithms for traffic sign recognition. *Neural Networks*, 32:323–332, 2012. ISSN 0893-6080. doi:
562 <https://doi.org/10.1016/j.neunet.2012.02.016>. URL <https://www.sciencedirect.com/science/article/pii/S0893608012000457>. Selected Papers from IJCNN 2011.

564 [87] Ziwei Liu, Ping Luo, Xiaogang Wang, and Xiaoou Tang. Deep learning face attributes in the wild. In
565 *Proceedings of the IEEE International Conference on Computer Vision (ICCV)*, December 2015.

566 [88] Michael Zhang, Nimit S Sohoni, Hongyang R Zhang, Chelsea Finn, and Christopher Ré. Correct-n-
567 contrast: A contrastive approach for improving robustness to spurious correlations. *arXiv preprint*
568 *arXiv:2203.01517*, 2022.

569 [89] Alex Krizhevsky, Geoffrey Hinton, et al. Learning multiple layers of features from tiny images. 2009.

570 [90] Olga Russakovsky, Jia Deng, Hao Su, Jonathan Krause, Sanjeev Satheesh, Sean Ma, Zhiheng Huang,
571 Andrej Karpathy, Aditya Khosla, Michael Bernstein, Alexander C. Berg, and Li Fei-Fei. ImageNet Large
572 Scale Visual Recognition Challenge. *International Journal of Computer Vision (IJCV)*, 115(3):211–252,
573 2015. doi: 10.1007/s11263-015-0816-y.

574 [91] Yonglong Tian, Dilip Krishnan, and Phillip Isola. Contrastive multiview coding. In *Computer Vision-
575 ECCV 2020: 16th European Conference, Glasgow, UK, August 23–28, 2020, Proceedings, Part XI 16*,
576 pages 776–794. Springer, 2020.

577 [92] William B Johnson. Extensions of lipshitz mapping into hilbert space. In *Conference modern analysis
578 and probability*, 1984, pages 189–206, 1984.

579 [93] Zeyu Zhao. The application of the right to be forgotten in the machine learning context: From the
580 perspective of european laws. *Cath. UJL & Tech*, 31:73, 2022.

581 [94] Sungjin Lim and Junhyoung Oh. Navigating privacy: A global comparative analysis of data protection
582 laws. *IET Information Security*, 2025(1):5536763, 2025.

583 [95] Angela M Lonzetta and Thaier Hayajneh. Challenges of complying with data protection and privacy
584 regulations. *EAI Endorsed Trans. Scalable Inf. Syst.*, 8(30):e4, 2021.

585 [96] Oskar J Gstrein and Anne Beaulieu. How to protect privacy in a datafied society? a presentation of
586 multiple legal and conceptual approaches. *Philosophy & Technology*, 35(1):3, 2022.

587 [97] Jiaxin Fan, Qi Yan, Mohan Li, Guanqun Qu, and Yang Xiao. A survey on data poisoning attacks and
588 defenses. In *2022 7th IEEE International Conference on Data Science in Cyberspace (DSC)*, pages
589 48–55. IEEE, 2022.

590 [98] Ram Shankar Siva Kumar, David R O’Brien, Kendra Albert, and Salome Vilojen. Law and adversarial
591 machine learning. *arXiv preprint arXiv:1810.10731*, 2018.

592 [99] Monty-Maximilian Zühlke and Daniel Kudenko. Adversarial robustness of neural networks from the
 593 perspective of lipschitz calculus: A survey. *ACM Computing Surveys*, 57(6):1–41, 2025.

594 [100] Gilad Cohen, Guillermo Sapiro, and Raja Giryes. Detecting adversarial samples using influence functions
 595 and nearest neighbors. In *Proceedings of the IEEE/CVF conference on computer vision and pattern
 596 recognition*, pages 14453–14462, 2020.

597 [101] Rabab Abdelfattah, Qing Guo, Xiaoguang Li, Xiaofeng Wang, and Song Wang. Cdul: Clip-driven
 598 unsupervised learning for multi-label image classification. In *Proceedings of the IEEE/CVF international
 599 conference on computer vision*, pages 1348–1357, 2023.

600 [102] Arthur Jacot, Franck Gabriel, and Clément Hongler. Neural tangent kernel: Conver-
 601 gence and generalization in neural networks. In *Advances in Neural Information Process-
 602 ing Systems*, volume 31, 2018. URL <https://proceedings.neurips.cc/paper/2018/file/5a4be1fa34b8f9b53d01fdd7c1dc38c1-Paper.pdf>.

604 [103] Greg Yang and Hadi Salman. A fine-grained spectral perspective on neural networks. *arXiv preprint
 605 arXiv:1907.10599*, 2019.

606 [104] Narine Kokhlikyan, Vivek Miglani, Miguel Martin, Edward Wang, Bilal Alsallakh, Jonathan Reynolds,
 607 Alexander Melnikov, Natalia Kliushkina, Carlos Araya, Siqi Yan, et al. Captum: A unified and generic
 608 model interpretability library for pytorch. *arXiv preprint arXiv:2009.07896*, 2020.

609 [105] Benedikt Boecking, Nicholas Roberts, Willie Neiswanger, Stefano Ermon, Frederic Sala, and Ar-
 610 tur Dubrawski. Generative modeling helps weak supervision (and vice versa). *arXiv preprint
 611 arXiv:2203.12023*, 2022.

612 [106] Olga Russakovsky and Li Fei-Fei. Attribute learning in large-scale datasets. In *European conference on
 613 computer vision*, pages 1–14. Springer, 2010.

614 [107] Alan Pham, Eunice Chan, Vikranth Srivatsa, Dhruba Ghosh, Yaoqing Yang, Yaodong Yu, Ruiqi Zhong,
 615 Joseph E Gonzalez, and Jacob Steinhardt. The effect of model size on worst-group generalization. *arXiv
 616 preprint arXiv:2112.04094*, 2021.

617 [108] Muxi Chen, YU LI, and Qiang Xu. Hibug: On human-interpretable model debug. In *Thirty-seventh
 618 Conference on Neural Information Processing Systems*, 2023. URL <https://openreview.net/forum?id=4sDHLxKb1L>.

620 **NeurIPS Paper Checklist**

621 **1. Claims**

622 Question: Do the main claims made in the abstract and introduction accurately reflect the paper's
623 contributions and scope?

624 Answer: [\[Yes\]](#)

625 Justification: The abstract and introduction clearly articulate the primary contributions of the paper.

626 Guidelines:

- 627 • The answer NA means that the abstract and introduction do not include the claims made in the
628 paper.
- 629 • The abstract and/or introduction should clearly state the claims made, including the contributions
630 made in the paper and important assumptions and limitations. A No or NA answer to this
631 question will not be perceived well by the reviewers.
- 632 • The claims made should match theoretical and experimental results, and reflect how much the
633 results can be expected to generalize to other settings.
- 634 • It is fine to include aspirational goals as motivation as long as it is clear that these goals are not
635 attained by the paper.

636 **2. Limitations**

637 Question: Does the paper discuss the limitations of the work performed by the authors?

638 Answer: [\[Yes\]](#)

639 Justification: The paper explicitly discusses the limitations of existing methods in the Conclusion
640 section, highlighting areas where current approaches fall short and talks about future research direction.

641 Guidelines:

- 642 • The answer NA means that the paper has no limitation while the answer No means that the paper
643 has limitations, but those are not discussed in the paper.
- 644 • The authors are encouraged to create a separate "Limitations" section in their paper.
- 645 • The paper should point out any strong assumptions and how robust the results are to violations of
646 these assumptions (e.g., independence assumptions, noiseless settings, model well-specification,
647 asymptotic approximations only holding locally). The authors should reflect on how these
648 assumptions might be violated in practice and what the implications would be.
- 649 • The authors should reflect on the scope of the claims made, e.g., if the approach was only tested
650 on a few datasets or with a few runs. In general, empirical results often depend on implicit
651 assumptions, which should be articulated.
- 652 • The authors should reflect on the factors that influence the performance of the approach. For
653 example, a facial recognition algorithm may perform poorly when image resolution is low or
654 images are taken in low lighting. Or a speech-to-text system might not be used reliably to provide
655 closed captions for online lectures because it fails to handle technical jargon.
- 656 • The authors should discuss the computational efficiency of the proposed algorithms and how
657 they scale with dataset size.
- 658 • If applicable, the authors should discuss possible limitations of their approach to address problems
659 of privacy and fairness.
- 660 • While the authors might fear that complete honesty about limitations might be used by reviewers
661 as grounds for rejection, a worse outcome might be that reviewers discover limitations that
662 aren't acknowledged in the paper. The authors should use their best judgment and recognize
663 that individual actions in favor of transparency play an important role in developing norms that
664 preserve the integrity of the community. Reviewers will be specifically instructed to not penalize
665 honesty concerning limitations.

666 **3. Theory assumptions and proofs**

667 Question: For each theoretical result, does the paper provide the full set of assumptions and a complete
668 (and correct) proof?

669 Answer: [\[Yes\]](#)

670 Justification: All assumptions and detailed proofs are provided in Appendix F.

671 Guidelines:

- 672 • The answer NA means that the paper does not include theoretical results.
- 673 • All the theorems, formulas, and proofs in the paper should be numbered and cross-referenced.
- 674 • All assumptions should be clearly stated or referenced in the statement of any theorems.

675 • The proofs can either appear in the main paper or the supplemental material, but if they appear in
 676 the supplemental material, the authors are encouraged to provide a short proof sketch to provide
 677 intuition.
 678 • Inversely, any informal proof provided in the core of the paper should be complemented by
 679 formal proofs provided in appendix or supplemental material.
 680 • Theorems and Lemmas that the proof relies upon should be properly referenced.

681 **4. Experimental result reproducibility**

682 Question: Does the paper fully disclose all the information needed to reproduce the main experimental
 683 results of the paper to the extent that it affects the main claims and/or conclusions of the paper
 684 (regardless of whether the code and data are provided or not)?

685 Answer: [\[Yes\]](#)

686 Justification: The codebase for reproducing the results is linked in the Abstract, and Appendix H
 687 provides additional implementation details.

688 Guidelines:

689 • The answer NA means that the paper does not include experiments.
 690 • If the paper includes experiments, a No answer to this question will not be perceived well by the
 691 reviewers: Making the paper reproducible is important, regardless of whether the code and data
 692 are provided or not.
 693 • If the contribution is a dataset and/or model, the authors should describe the steps taken to make
 694 their results reproducible or verifiable.
 695 • Depending on the contribution, reproducibility can be accomplished in various ways. For
 696 example, if the contribution is a novel architecture, describing the architecture fully might suffice,
 697 or if the contribution is a specific model and empirical evaluation, it may be necessary to either
 698 make it possible for others to replicate the model with the same dataset, or provide access to
 699 the model. In general, releasing code and data is often one good way to accomplish this, but
 700 reproducibility can also be provided via detailed instructions for how to replicate the results,
 701 access to a hosted model (e.g., in the case of a large language model), releasing of a model
 702 checkpoint, or other means that are appropriate to the research performed.
 703 • While NeurIPS does not require releasing code, the conference does require all submissions
 704 to provide some reasonable avenue for reproducibility, which may depend on the nature of the
 705 contribution. For example
 706 (a) If the contribution is primarily a new algorithm, the paper should make it clear how to
 707 reproduce that algorithm.
 708 (b) If the contribution is primarily a new model architecture, the paper should describe the
 709 architecture clearly and fully.
 710 (c) If the contribution is a new model (e.g., a large language model), then there should either be
 711 a way to access this model for reproducing the results or a way to reproduce the model (e.g.,
 712 with an open-source dataset or instructions for how to construct the dataset).
 713 (d) We recognize that reproducibility may be tricky in some cases, in which case authors are
 714 welcome to describe the particular way they provide for reproducibility. In the case of
 715 closed-source models, it may be that access to the model is limited in some way (e.g.,
 716 to registered users), but it should be possible for other researchers to have some path to
 717 reproducing or verifying the results.

718 **5. Open access to data and code**

719 Question: Does the paper provide open access to the data and code, with sufficient instructions to
 720 faithfully reproduce the main experimental results, as described in supplemental material?

721 Answer: [\[Yes\]](#)

722 Justification: The codebase for reproducing the results is linked in the Abstract, and Appendix H
 723 provides additional implementation details.

724 Guidelines:

725 • The answer NA means that paper does not include experiments requiring code.
 726 • Please see the NeurIPS code and data submission guidelines (<https://nips.cc/public/guides/CodeSubmissionPolicy>) for more details.
 727 • While we encourage the release of code and data, we understand that this might not be possible,
 728 so “No” is an acceptable answer. Papers cannot be rejected simply for not including code, unless
 729 this is central to the contribution (e.g., for a new open-source benchmark).
 730 • The instructions should contain the exact command and environment needed to run to reproduce
 731 the results. See the NeurIPS code and data submission guidelines (<https://nips.cc/public/guides/CodeSubmissionPolicy>) for more details.

734 • The authors should provide instructions on data access and preparation, including how to access
 735 the raw data, preprocessed data, intermediate data, and generated data, etc.
 736 • The authors should provide scripts to reproduce all experimental results for the new proposed
 737 method and baselines. If only a subset of experiments are reproducible, they should state which
 738 ones are omitted from the script and why.
 739 • At submission time, to preserve anonymity, the authors should release anonymized versions (if
 740 applicable).
 741 • Providing as much information as possible in supplemental material (appended to the paper) is
 742 recommended, but including URLs to data and code is permitted.

743 **6. Experimental setting/details**

744 Question: Does the paper specify all the training and test details (e.g., data splits, hyperparameters,
 745 how they were chosen, type of optimizer, etc.) necessary to understand the results?

746 Answer: [\[Yes\]](#)

747 Justification: The aforementioned details are available in Appendix H.

748 Guidelines:

- 749 • The answer NA means that the paper does not include experiments.
- 750 • The experimental setting should be presented in the core of the paper to a level of detail that is
 751 necessary to appreciate the results and make sense of them.
- 752 • The full details can be provided either with the code, in appendix, or as supplemental material.

753 **7. Experiment statistical significance**

754 Question: Does the paper report error bars suitably and correctly defined or other appropriate information
 755 about the statistical significance of the experiments?

756 Answer: [\[Yes\]](#)

757 Justification: The mean across three runs is reported in the main draft.

758 Guidelines:

- 759 • The answer NA means that the paper does not include experiments.
- 760 • The authors should answer "Yes" if the results are accompanied by error bars, confidence
 761 intervals, or statistical significance tests, at least for the experiments that support the main claims
 762 of the paper.
- 763 • The factors of variability that the error bars are capturing should be clearly stated (for example,
 764 train/test split, initialization, random drawing of some parameter, or overall run with given
 765 experimental conditions).
- 766 • The method for calculating the error bars should be explained (closed form formula, call to a
 767 library function, bootstrap, etc.)
- 768 • The assumptions made should be given (e.g., Normally distributed errors).
- 769 • It should be clear whether the error bar is the standard deviation or the standard error of the
 770 mean.
- 771 • It is OK to report 1-sigma error bars, but one should state it. The authors should preferably report
 772 a 2-sigma error bar than state that they have a 96% CI, if the hypothesis of Normality of errors is
 773 not verified.
- 774 • For asymmetric distributions, the authors should be careful not to show in tables or figures
 775 symmetric error bars that would yield results that are out of range (e.g. negative error rates).
- 776 • If error bars are reported in tables or plots, The authors should explain in the text how they were
 777 calculated and reference the corresponding figures or tables in the text.

778 **8. Experiments compute resources**

779 Question: For each experiment, does the paper provide sufficient information on the computer
 780 resources (type of compute workers, memory, time of execution) needed to reproduce the experiments?

781 Answer: [\[Yes\]](#)

782 Justification: Memory and time complexities are reported in Appendix S and Appendix R, respectively.
 783 Additional details can be found in the Experiments section.

784 Guidelines:

- 785 • The answer NA means that the paper does not include experiments.
- 786 • The paper should indicate the type of compute workers CPU or GPU, internal cluster, or cloud
 787 provider, including relevant memory and storage.

788 • The paper should provide the amount of compute required for each of the individual experimental
789 runs as well as estimate the total compute.
790 • The paper should disclose whether the full research project required more compute than the
791 experiments reported in the paper (e.g., preliminary or failed experiments that didn't make it into
792 the paper).

793 **9. Code of ethics**

794 Question: Does the research conducted in the paper conform, in every respect, with the NeurIPS Code
795 of Ethics <https://neurips.cc/public/EthicsGuidelines>?

796 Answer: [\[Yes\]](#)

797 Justification: Most ethical concerns are either not applicable to this work or have been appropriately
798 addressed.

799 Guidelines:

800 • The answer NA means that the authors have not reviewed the NeurIPS Code of Ethics.
801 • If the authors answer No, they should explain the special circumstances that require a deviation
802 from the Code of Ethics.
803 • The authors should make sure to preserve anonymity (e.g., if there is a special consideration due
804 to laws or regulations in their jurisdiction).

805 **10. Broader impacts**

806 Question: Does the paper discuss both potential positive societal impacts and negative societal impacts
807 of the work performed?

808 Answer: [\[NA\]](#)

809 Justification: This work does not pose any specific societal risks; on the contrary, the proposed method
810 actively addresses and mitigates model biases.

811 Guidelines:

812 • The answer NA means that there is no societal impact of the work performed.
813 • If the authors answer NA or No, they should explain why their work has no societal impact or
814 why the paper does not address societal impact.
815 • Examples of negative societal impacts include potential malicious or unintended uses (e.g.,
816 disinformation, generating fake profiles, surveillance), fairness considerations (e.g., deploy-
817 ment of technologies that could make decisions that unfairly impact specific groups), privacy
818 considerations, and security considerations.
819 • The conference expects that many papers will be foundational research and not tied to particular
820 applications, let alone deployments. However, if there is a direct path to any negative applications,
821 the authors should point it out. For example, it is legitimate to point out that an improvement in
822 the quality of generative models could be used to generate deepfakes for disinformation. On the
823 other hand, it is not needed to point out that a generic algorithm for optimizing neural networks
824 could enable people to train models that generate Deepfakes faster.
825 • The authors should consider possible harms that could arise when the technology is being used
826 as intended and functioning correctly, harms that could arise when the technology is being used
827 as intended but gives incorrect results, and harms following from (intentional or unintentional)
828 misuse of the technology.
829 • If there are negative societal impacts, the authors could also discuss possible mitigation strategies
830 (e.g., gated release of models, providing defenses in addition to attacks, mechanisms for monitor-
831 ing misuse, mechanisms to monitor how a system learns from feedback over time, improving the
832 efficiency and accessibility of ML).

833 **11. Safeguards**

834 Question: Does the paper describe safeguards that have been put in place for responsible release of
835 data or models that have a high risk for misuse (e.g., pretrained language models, image generators, or
836 scraped datasets)?

837 Answer: [\[NA\]](#)

838 Justification: This work does not pose any such risks.

839 Guidelines:

840 • The answer NA means that the paper poses no such risks.
841 • Released models that have a high risk for misuse or dual-use should be released with necessary
842 safeguards to allow for controlled use of the model, for example by requiring that users adhere to
843 usage guidelines or restrictions to access the model or implementing safety filters.

844 • Datasets that have been scraped from the Internet could pose safety risks. The authors should
845 describe how they avoided releasing unsafe images.
846 • We recognize that providing effective safeguards is challenging, and many papers do not require
847 this, but we encourage authors to take this into account and make a best faith effort.

848 **12. Licenses for existing assets**

849 Question: Are the creators or original owners of assets (e.g., code, data, models), used in the paper,
850 properly credited and are the license and terms of use explicitly mentioned and properly respected?

851 Answer: [Yes]

852 Justification: Our code provides credit to external codebases in github repository.

853 Guidelines:

854 • The answer NA means that the paper does not use existing assets.
855 • The authors should cite the original paper that produced the code package or dataset.
856 • The authors should state which version of the asset is used and, if possible, include a URL.
857 • The name of the license (e.g., CC-BY 4.0) should be included for each asset.
858 • For scraped data from a particular source (e.g., website), the copyright and terms of service of
859 that source should be provided.
860 • If assets are released, the license, copyright information, and terms of use in the package should
861 be provided. For popular datasets, paperswithcode.com/datasets has curated licenses for
862 some datasets. Their licensing guide can help determine the license of a dataset.
863 • For existing datasets that are re-packaged, both the original license and the license of the derived
864 asset (if it has changed) should be provided.
865 • If this information is not available online, the authors are encouraged to reach out to the asset's
866 creators.

867 **13. New assets**

868 Question: Are new assets introduced in the paper well documented and is the documentation provided
869 alongside the assets?

870 Answer: [NA]

871 Justification: We have not introduced any new assets in this work.

872 Guidelines:

873 • The answer NA means that the paper does not release new assets.
874 • Researchers should communicate the details of the dataset/code/model as part of their sub-
875 missions via structured templates. This includes details about training, license, limitations,
876 etc.
877 • The paper should discuss whether and how consent was obtained from people whose asset is
878 used.
879 • At submission time, remember to anonymize your assets (if applicable). You can either create an
880 anonymized URL or include an anonymized zip file.

881 **14. Crowdsourcing and research with human subjects**

882 Question: For crowdsourcing experiments and research with human subjects, does the paper include
883 the full text of instructions given to participants and screenshots, if applicable, as well as details about
884 compensation (if any)?

885 Answer: [NA]

886 Justification: No crowdsourcing-based experiments were conducted in this work.

887 Guidelines:

888 • The answer NA means that the paper does not involve crowdsourcing nor research with human
889 subjects.
890 • Including this information in the supplemental material is fine, but if the main contribution of the
891 paper involves human subjects, then as much detail as possible should be included in the main
892 paper.
893 • According to the NeurIPS Code of Ethics, workers involved in data collection, curation, or other
894 labor should be paid at least the minimum wage in the country of the data collector.

895 **15. Institutional review board (IRB) approvals or equivalent for research with human subjects**

896 Question: Does the paper describe potential risks incurred by study participants, whether such
897 risks were disclosed to the subjects, and whether Institutional Review Board (IRB) approvals (or an
898 equivalent approval/review based on the requirements of your country or institution) were obtained?

Answer: [NA]

Justification: No experiments involving human subjects were conducted for this work

Guidelines:

- The answer NA means that the paper does not involve crowdsourcing nor research with human subjects.
- Depending on the country in which research is conducted, IRB approval (or equivalent) may be required for any human subjects research. If you obtained IRB approval, you should clearly state this in the paper.
- We recognize that the procedures for this may vary significantly between institutions and locations, and we expect authors to adhere to the NeurIPS Code of Ethics and the guidelines for their institution.
- For initial submissions, do not include any information that would break anonymity (if applicable), such as the institution conducting the review.

16. Declaration of LLM usage

Question: Does the paper describe the usage of LLMs if it is an important, original, or non-standard component of the core methods in this research? Note that if the LLM is used only for writing, editing, or formatting purposes and does not impact the core methodology, scientific rigorousness, or originality of the research, declaration is not required.

Answer: [Yes]

Justification: Our work builds on the approach proposed by HiBug [39] and leverages large language models (LLMs) and vision-language models (VLMs) for data annotation.

Guidelines:

- The answer NA means that the core method development in this research does not involve LLMs as any important, original, or non-standard components.
- Please refer to our LLM policy (<https://neurips.cc/Conferences/2025/LLM>) for what should or should not be described.

Algorithm 1 Proposed Method

Require: Training Dataset ($\mathcal{D}_{\text{train}}$), Validation Dataset ($\mathcal{D}_{\text{valid}}$), Number of Checkpoints (M), Rank for Metric Learning (t), Min Weight Fraction (β), Cutoff for Subset Selection (γ), CLIP Embedding Model (\mathcal{C}), Epochs for Classifier Training (\mathcal{E}), Optimization Iterations for Metric Learning (\mathcal{I}).

- 1: **## Classifier Training**
- 2: **i=0**
- 3: **for** epoch $\in [0 \dots \mathcal{E}]$ **do**
- 4: Train the classifier using $\mathcal{D}_{\text{train}}$.
- 5: **if** epoch $\in [\mathcal{E}, \mathcal{E} - 2, \mathcal{E} - 4, \mathcal{E} - 6, \mathcal{E} - 8]$ **then**
- 6: Save the checkpoint θ_i .
- 7: **i+=1**
- 8: **end if**
- 9: **end for**
- 10: Save $N = [\theta_0, \theta_1, \theta_2, \theta_3, \theta_4]$ checkpoints for the calculation of attribution score as per Equation 4.
- 11: **## Spurious Feature Identification**
- 12: Generate a list of possible attributes and corresponding values for $\mathcal{D}_{\text{valid}}$ using ChatGPT (Section 3.2).
- 13: **for** $i \in [1 \dots |\mathcal{D}_{\text{val}}|]$ **do**
- 14: Annotate attribute-value pairs for sample v_i using a Llama-based VLM model (Section 3.2).
- 15: **end for**
- 16: **## Calculating the Detrimental Attribution Score**
- 17: **for** $z_i \in \{z_1 \dots z_n\}$ **do**
- 18: Calculate the attribution score $\mathcal{A}(z_i)$ using the saved checkpoints (Equations 4 and 5).
- 19: **end for**
- 20: Compare the accuracy of each attribute-value pair using Equation 1. Flag an attribute-value pair as spurious if its accuracy exceeds the average dataset accuracy by a threshold τ .
- 21: Generate a textual representation of flagged attribute-value pairs under the context of the dataset (Appendix H.4).
- 22: Create a CLIP embedding of the textual representation ($\mathcal{C}_{\text{text}}$).
- 23: **## Metric Learning**
- 24: **for** $i \in [1 \dots |\mathcal{D}_{\text{train}}|]$ **do**
- 25: Calculate the CLIP image embedding ($\mathcal{C}_{\text{image}}^i$) for each sample z_i in $\mathcal{D}_{\text{train}}$.
- 26: **end for**
- 27: **for** $i \in [0 \dots \mathcal{I}]$ **do**
- 28: Optimize the loss \mathcal{L} using $\mathcal{C}_{\text{text}}$, $\mathcal{C}_{\text{image}}$, and $\mathcal{A}(z)$ as per Equation 10 to generate the metric \mathbf{k} using the hyperparameter t, β .
- 29: **end for**
- 30: Use the score \mathbf{k}, γ to identify $\mathcal{S}^{\text{deter}}$ and retrain the model on $\mathcal{D}_{\text{train}} \setminus \mathcal{S}^{\text{deter}}$.

$$\alpha(v_j, z_i) = \frac{1}{N} \sum_{n=1}^N \left(\phi_n(v_j)^\top (\Phi_n^\top \Phi_n)^{-1} \phi_n(z_i) \right) \times \frac{1}{N} \sum_{n=1}^N \left(1 - p_n^{z_i} \right)$$

where, $p_n^{z_i} = (1 + \exp(-y_i \mathbf{f}(x_i; \theta_n^*)))^{-1}$, $\phi_n(v_j) = \mathcal{P}^\top \nabla_{\theta} \mathbf{f}(v_j; \theta_n^*)$,
 $\phi_n(z_i) = \mathcal{P}^\top \nabla_{\theta} \mathbf{f}(z_i; \theta_n^*)$, $\Phi_n = [\phi_n(z_1)^\top; \dots; \phi_n(z_{|\mathcal{D}_{\text{train}}|})^\top]$
 $\Phi_n \in \mathbb{R}^{m \times k}$, $\mathcal{P} \sim \mathcal{N}(0, 1)^{p \times k}$, $k \ll p$. (8)

927 Equation 8, illustrates the calculation of the trak score. Scores consist of an average of the data attribution score
928 calculated over multiple checkpoints (N). The terms $\phi_n(v_j)$ and $\phi_n(z_i)$ denote the projected gradients of the
929 validation sample v_j and the training sample z_i for the n^{th} set of parameters and projection matrix \mathcal{P} . This
930 projection matrix reduces the dimension of the gradient $\nabla_{\theta} \mathbf{f}(z; \theta_n^*) \in \mathbb{R}^p$ to a lower-dimensional space \mathbb{R}^k ,
931 where $k \ll p$, while approximately preserving the inner product, as per the classical Johnson-Lindenstrauss
932 theorem [92].

933 C Soft Penalty for Optimization

934 For efficient optimisation of the constrained objective presented in Equation 7, we have replaced the hard
 935 constraint with a soft constraint ($d(k)$) as per d'Eon et al. [83].

$$d(k) = C \cdot \max \left(\frac{\left(\sum_{i=1}^{|D_{\text{train}}|} k_i - (\mathcal{T} + w) \right)^2}{w^2}, 0 \right), \quad (9)$$

936 This penalty term is quadratic and scaled by a shrinkable weight w , which is gradually reduced throughout the
 937 optimization process. The overall unconstrained optimization problem is defined in Equation 10 where C is a
 938 hyperparameter.

$$\mathcal{L} = \max_L \sum_{i=1}^{|D_{\text{train}}|} \left(\frac{k_i}{\sum_j k_j} \right) \mathcal{A}(z_i) - d(k). \quad (10)$$

939 D Notations

Table 7: Notation table for key equation in main draft and proof

Symbol	Description
General Definitions	
$h(x)$	Model prediction for input x
y	True label corresponding to input x
$\mathbf{1}(h(x) = y)$	Indicator function: 1 if prediction is correct, else 0
D_{val}	Validation dataset
$D_{(a^v, b_j^v)}$	Subset of validation data with attribute-value pair (a^v, b_j^v)
D_{train}	Training dataset: $D_{\text{train}} = \{z_1, z_2, \dots, z_n\}$ where $z_i = (x_i, y_i)$
\mathcal{X}, \mathcal{Y}	Feature set $\mathcal{X} = \{x_1, x_2, \dots, x_n\}$ and label set $\mathcal{Y} = \{y_1, y_2, \dots, y_n\}$
z_k, z_i	Training samples from D_{train}
v_j	Validation sample
\hat{y}	Output of the final logit layer of a neural network
θ	Vectorized parameters of the neural network, $\theta \in \mathbb{R}^p$
e_i	Standard unit vectors
Neural Tangent Kernel (NTK) Specific	
$\mathcal{G}(\mathcal{X}, \theta)$	Neural Tangent Random Feature (NTRF) matrix: $\mathcal{G} = \frac{\partial \hat{y}(\mathcal{X}; \theta)}{\partial \theta}$
\mathcal{G}_0	NTRF matrix at initialization: $\mathcal{G}_0 = \mathcal{G}(\mathcal{X}, \theta_0)$
SVD Decomposition and Gradient Starvation	
U, S, V	Singular Value Decomposition (SVD) components: $Y \mathcal{G}_0 = USV^T$
u^i, v_k	Singular vectors from U and V corresponding to features
s_i	Singular value representing the strength of the i^{th} feature
Γ	Response of the network to features: $\Gamma = U^T Y \hat{y} = SV^T \theta$
Γ_i	Response of the i^{th} feature
Attribution and Trak Scoring	
Φ_n	Stacked gradient features of all training points for model n
$f(v; \theta)$	Model output used for attribution (e.g., logit or loss) for input v under parameters θ
$\phi_n(\cdot)$	Projected gradient feature under model n
$\alpha(v_j, z_i)$	Attribution score: impact of removing z_i on prediction for v_j
$\mathcal{A}(z_i)$	Detrimental attribution score for training sample z_i
$p_n^{z_i}$	Predicted probability for z_i under model n
\mathcal{P}	Random projection matrix with entries drawn from $\mathcal{N}(0, 1)$
Optimization and others	
$\mathcal{C}_{\text{text}}, \mathcal{C}_{\text{image}}^i$	Text and image embeddings respectively
\mathcal{T}	Trade-off hyperparameter: $\mathcal{T} = \beta \times D_{\text{train}} $ (control tradeoff between data attribution and semantic coherence)
β	Hyperparameter associated with \mathcal{T}
k_i	Selection weight for sample i
$d(k)$	Penalty term enforcing deletion constraint
\mathcal{L}	Final optimization objective including penalty
C	Hyperparameter associated with soft penalty Equation 9
$M = LL^T$	Metric matrix constructed from L
$L \in \mathbb{R}^{D \times t}$	Learnable matrix under optimization defined by Equation 7
τ	Accuracy threshold to detect spurious bias
$\theta^*(\cdot)$	Final model parameters trained on the specified dataset

940 E Methods for Handling Spurious Features

941 Table 8 outlines the key capabilities and limitations of existing methods relative to ours. While data augmentation
 942 techniques [62–67] are widely adopted, they often require external data, which can conflict with privacy and
 943 regulatory constraints [93–96]. Moreover, without appropriate supervision, they risk introducing new spurious
 944 features or being vulnerable to data poisoning attacks [97, 98].

945 In contrast, methods such as group annotation-based optimization (e.g., gDRO [17]), loss reweighting techniques
946 (e.g., JTT [16]), and final-layer fine-tuning [70, 20] do not pose privacy risks. However, in safety-critical
947 applications where models must satisfy stability guarantees [75, 76, 99], these methods can compromise
948 robustness, especially when models are required to ensure Lipschitz continuity for certification. Specifically,
949 they are susceptible to targeted attacks [21–24], particularly when the training procedure heavily relies on a
950 small subset of influential examples [100, 98] used for fine-tuning or reweighting loss values.
951 Group-balancing techniques [28, 29] partially address these challenges, but often over-prune majority groups. In
952 contrast, our method supports budget-constrained, targeted sample removal, ensuring only detrimental examples
953 are excluded during training.
954 Furthermore, many of these methods [17, 28, 29] rely on manual group annotations of the training dataset. As
955 spurious features [77] evolve post-deployment, maintaining robustness would require repeated manual annotation
956 cycles. In contrast, our approach eliminates the need for group labels for the training dataset and leverages
957 textual descriptions of bias to guide targeted data removal. The use of a textual description of the bias and
958 the proposed metric learning approach provides a zero-shot approach [101, 82] to approximate the underlying
959 group structure without having any annotation overhead. This design also allows integration of feedback from
960 subject-matter experts, making the process more adaptive and practical.

Table 8: Comparison of methods across regulatory and robustness capabilities.

Method	Regulatory Restrictions	Supports Textual Descriptions	No Group Annotation in Training Data	Privacy	Prevent Over pruning of Majority Group	Robust to Adv-Attacks
Data Augmentation	✗	✗	✓	✗	✓	✗
Group-Annotation based Optimization	✗	✗	✗	✓	✓	-
Reweighting Loss/Data	✗	✗	✓	✓	✓	✗
Last Layer Fine-Tuning	✗	✗	✓	✓	✓	✗
Group Balancing Method	✓	✗	✗	✓	✗	✓
Ours	✓	✓	✓	✓	✓	✓

961 F Theoretical Formulation

962 For dataset $\mathcal{D}_{\text{train}} = \{z_1 \dots z_n\}$ where $z_i = (x_i, y_i)$, and $x_i \in \mathbb{R}^d$, and corresponding labels $y_i \in \{-1, +1\}^n$.
963 Let \hat{y} denotes the output of the final logit layer of an L-layer neural network trained using binary cross-entropy,
964 and $\theta \in \mathbb{R}^p$ represents a p-dimensional vectorized parameter of the neural network (Equation 4, Equation 8). let
965 $\mathcal{X} = \{x_1 \dots x_n\}$ and $\mathcal{Y} = \{y_1 \dots y_n\}$ constitute the respective features and class labels.
966 In the Neural Tangent Kernel (NTK) framework [102], the final output of a neural network can be approximated
967 as a linear function of parameters, whose properties are governed by the Neural Tangent Random Feature (NTRF)
968 matrix, defined as:

$$\mathcal{G}(\mathcal{X}, \theta) = \frac{\partial \hat{y}(\mathcal{X}; \theta)}{\partial \theta}, \quad \mathcal{G} \in \mathbb{R}^{n \times p}. \quad (11)$$

969 For wide-width neural networks, the NTRF matrix remains approximately constant during training [61], allowing
970 the output of the neural network to be approximated using the initial NTRF matrix, $\mathcal{G}_0 = \mathcal{G}(\mathcal{X}, \theta_0)$, as follows:

$$\hat{y}(\mathcal{X}, \theta) = \mathcal{G}_0 \theta. \quad (12)$$

971 The dominant features of the dataset can be estimated using the principal components of $\mathcal{G}_0 = \mathcal{G}(\mathcal{X}, \theta_0)$, which
972 are equivalent to the principal components of the NTK gram matrix [103].
973 **Definition 2** (Features and gradient starvation [61]). *Consider a support vector decomposition of $Y\mathcal{G}_0 =$
974 USV^\top , where $Y = \text{diag}(y)$, the i^{th} feature is represented by $(V^\top)_{(i,:)}$ or $(V)_{(:,i)}$ with its strength denoted
975 as $s_i = (S)_{ii}$ and its weight across all training samples represented by $(U)_{(:,i)}$. The response of the neural
976 network to the i^{th} feature can be expressed as Γ_i , where:*

$$\Gamma := U^\top Y \hat{y} = SV^\top \theta.$$

977 Due to the imbalance in the training dataset, for a given set of features and the optimal parameter θ^* , the
978 presence of the i^{th} feature can influence the learning of the j^{th} feature. This phenomenon, referred to as gradient
979 starvation, arises in optimal parameters if:

$$\frac{d\Gamma_j^*}{d(s_i^2)} < 0$$

980 Definition 2 suggests that as the strength of the i^{th} feature (s_i^2) increases, the learning of the j^{th} feature gets
 981 impacted. This implies that stronger features can dominate the learning process, leading to a reduced contribution
 982 of other informative features in the model's predictions.

983 **Theorem 1** (Gradient Starvation Regime [61]). *For a neural network in the linear regime and trained using
 984 binary cross entropy loss with feature coupling between two features f_1 and f_2 as defined in Pezeshki et al. [61]
 985 and with $s_1^2 > s_2^2$, we have,*

$$\frac{d\Gamma_2^*}{d(s_1^2)} < 0,$$

986 Now, under the given setting, we will try to understand the influence of gradient starvation on the performance
 987 of the NTK-based data attribution methods :

988 **Proposition 2** (Under Valuation of Trak Scores). *Consider a neural network in the neural tangent kernel (NTK)
 989 regime, trained using binary cross-entropy loss with two equally informative features, f_1 and f_2 , lets assume
 990 that due to learning dynamics f_1 becomes dominant and cause gradient starvation of f_2 as per Pezeshki et al.
 991 [61]. Then, for two training samples z_i and z_j with equal representation of dominating features f_1 and f_2
 992 respectively. The attribution score for z_i can be systematically undervalued relative to z_j . Formally:*

$$|\mathcal{A}(z_i)| < |\mathcal{A}(z_j)|$$

993 *Proof.* For a sigmoid-based activation, the output probability for feature set (\mathcal{X}) is given by:

$$\begin{aligned} p(\mathcal{X}; \theta) &= \frac{1}{1 + \exp(-\hat{y}(\mathcal{X}; \theta))}, \\ p(\mathcal{X}; \theta) \cdot (1 + \exp(-\hat{y}(\mathcal{X}; \theta))) &= 1, \\ p(\mathcal{X}; \theta) \cdot \exp(-\hat{y}(\mathcal{X}; \theta)) &= 1 - p(\mathcal{X}; \theta), \\ \hat{y}(\mathcal{X}; \theta) &= \log\left(\frac{p(\mathcal{X}; \theta)}{1 - p(\mathcal{X}; \theta)}\right). \end{aligned} \tag{13}$$

994 Hence, the utility function (f) used in Trak for data attribution (Equation 3) is equivalent to the logit of a binary
 995 cross entropy (\hat{y}).

996 From the definition of gradients:

$$\frac{\partial \hat{y}(x; \theta)}{\partial \theta} = \frac{\partial \mathcal{G}_0 \cdot \theta}{\partial \theta} = \mathcal{G}_0 \tag{14}$$

997 As per Equation 4 and Equation 8, $\Phi_m = \mathcal{G}_0 \cdot \mathcal{P}$. Now, considering that the projection matrix [92] preserves
 998 the inner product of the actual gradient vector. We will simplify our argument and calculate the value for the
 999 unprojected gradients [32] ($\mathcal{P} = I_d$). Furthermore, under the NTK regime, where the optimal parameters are
 1000 similar [102], we calculate the attribution score for a single checkpoint (M=1). For ease of derivation, we will
 1001 omit the subscript m i.e., $\Phi_1 = \Phi$ and $\phi_1 = \phi$, hence:

$$\Phi = \mathcal{G}_0 \tag{15}$$

$$\Phi^T \Phi = \mathcal{G}_0^T \mathcal{G}_0 \tag{16}$$

1002 Now, as per the feature decomposition defined in Definition 2 :

$$\begin{aligned} Y\mathcal{G}_0 &= USV^\top \\ (Y\mathcal{G}_0)^\top (Y\mathcal{G}_0) &= \left(USV^\top\right)^\top \left(USV^\top\right) \\ \mathcal{G}_0^T Y^\top Y\mathcal{G}_0 &= VS^2V^T \end{aligned} \tag{17}$$

1003 Since $Y = \text{diag}\{y_1, \dots, y_n\}$ and $y \in \{-1, 1\}$, it follows that:

$$\begin{aligned} Y^T Y &= I, \\ \mathcal{G}_0^T \mathcal{G}_0 &= VS^2V^T, \\ \Phi^T \Phi &= VS^2V^T. \end{aligned} \tag{18}$$

1004 The validation attribution score (Equation 5) is given by :

$$\begin{aligned}
 \mathcal{A}(z_i) &= \sum_{v_j \in \mathcal{D}_{val}} -\alpha(v_j; z_i) \\
 &= \sum_{v_j \in \mathcal{D}_{val}} -\phi(v_j)^\top (\Phi^\top \Phi)^{-1} \phi(z_i) (1 - p^{z_i})
 \end{aligned} \tag{19}$$

1005 Substituting the value of $\Phi^\top \Phi$:

$$\begin{aligned}
 \mathcal{A}(z_i) &= \sum_{v_j \in \mathcal{D}_{val}} -\phi(v_j)^\top (VS^2V^\top)^{-1} \phi(z_i) (1 - p^{z_i}) \\
 &= \left(\sum_{v_j \in \mathcal{D}_{val}} -\phi(v_j)^\top \right) (V)^{-1}^\top S^{-2} (V)^{-1} \phi(z_i) (1 - p^{z_i}) \\
 &= \left(\sum_{v_j \in \mathcal{D}_{val}} -\phi(v_j)^\top \right) VS^{-2} V^\top \phi(z_i) (1 - p^{z_i}) \\
 &= \left(\sum_{v_j \in \mathcal{D}_{val}} -\nabla_\theta f(v_j, \theta)^\top \right) VS^{-2} V^\top \nabla_\theta f(z_i, \theta) (1 - p^{z_i}) \text{ (since } \mathcal{P} = I \text{ and as per Equation 8)} \\
 &= \left(\sum_{v_j \in \mathcal{D}_{val}} -\nabla_\theta f(v_j, \theta)^\top \right) VS^{-2} V^\top \nabla_\theta f(z_i, \theta) (1 - p^{z_i}) \\
 &= \sum_k \frac{\left(\left(\sum_{v_j \in \mathcal{D}_{val}} -\nabla_\theta f(v_j, \theta)^\top \right) v_k \right) \left(v_k^\top \nabla_\theta f(z_i, \theta) (1 - p^{z_i}) \right)}{s_{kk}^2}
 \end{aligned} \tag{20}$$

1006 where, v_k is the k^{th} column of V matrix and representing the k^{th} feature as per Definition 2

1007 now given the definition of the \mathcal{G}_0 and as per Equation 8, Equation 13 and Equation 15

$$\begin{aligned}
 \mathcal{G}_0 &= [\nabla_\theta f(z_1, \theta)^\top; \dots; \nabla_\theta f(z_n, \theta)^\top] \\
 Y\mathcal{G}_0 &= USV^\top
 \end{aligned} \tag{21}$$

1008 For the i^{th} training sample, this score can be further simplified by multiplying with the standard unit vector (e_i)
1009 on both sides:

$$\begin{aligned}
 e_i^\top Y\mathcal{G}_0 &= e_i^\top USV^\top \\
 y_i \nabla_\theta f(z_i, \theta)^\top &= u^i SV^\top
 \end{aligned} \tag{22}$$

1010 where u^i is a row vector associated with matrix U,

1011 multiplying both side with y_i and V we get ,

$$y_i \cdot y_i \nabla_\theta f(z_i, \theta)^\top V = y_i u^i S$$

1012 as $y_i^2 = 1$ and further multiplying both side with e_k we get

$$\begin{aligned}
 \nabla_\theta f(z_i, \theta)^\top V \cdot e_k &= y_i u^i S \cdot e_k \\
 \nabla_\theta f(z_i, \theta)^\top v_k &= y_i u_k^i s_{kk}
 \end{aligned} \tag{23}$$

1013 substituting the value in Equation 20 gives :

$$|\mathcal{A}(z_i)| = \left| \sum_k \frac{\left(\sum_{v_j \in \mathcal{D}_{val}} -\nabla_\theta f(v_j, \theta)^\top \right) v_k y_i u_k^i (1 - p^{z_i})}{s_{kk}} \right| \tag{24}$$

1014 According to the given equation, for any two data points z_i and z_j where the dominant features are f_1 and f_2
1015 respectively, the contribution of these features, as per Definition 2, is represented by u_1^i and u_2^j . When both
1016 dominant features are equally represented, it follows that $u_1^i = u_2^j$ and $u_1^i < u_2^j$, $u_2^j < u_1^i$. Furthermore, if
1017 $|s_{11}| > |s_{22}|$ then as per Theorem 1 f_1 induces gradient starvation of f_2 and results in lower attribution score
1018 i.e., $|\mathcal{A}(z_i)| < |\mathcal{A}(z_j)|$. \square

1019 **G Data Annotation**1020 **G.1 Attribute Generation**

1021 We utilize ChatGPT to generate attributes for a specific dataset with the following prompt referenced from
 1022 HiBug [39]. The list of attribute-value pairs generated by ChatGPT is provided in Table 9.

1023 *You are a helpful assistant to help user work on improving AI visual models. You need to discuss with your user
 1024 for a description of the task that the model is working for. You need to decide if the description is complete
 1025 and clear enough. The description should at least contains or infer the task object, task type, task scene. After
 1026 understanding user's task description, you should generate related visual attributes that might affect the model's
 1027 performance. You should not ask me to provide visual attributes. (Note that this is only an example visual
 1028 attributes according to the previous example, do not take any of its values as default value!): "Gender, Age
 1029 , Hairstyle , Hair colour" If user is satisfied with the attributes, generate the attribute form with the header
 1030 formatted as "//Attribute Form//" and end with "//END//". Attributes in the form should be spited by comma. Do
 1031 not include the task object, task type, task scene. (Note that this is only an example visual attributes according to
 1032 the previous example, do not take any of its values as default value!):
 1033 //Attribute Form// Gender , Age , Hairstyle , Hair colour //END//*

Table 9: Details of the attribute value pair generated using ChatGPT.

Dataset	Attributes	Choices
AWA2	Size of the Animal	Small, Medium, Large, Very Large
	Fur or Skin Texture of Animals	Smooth, Rough, Furry, Scaly
	Color Pattern on Animal	Striped, Spotted, Solid Color, Mixed Colors
	Posture of Animal	Sitting, Standing, Flying, Running
	Visible Markings or Patterns	Scars, Spots, Unique Patterns
	Lighting Conditions	Bright, Dim, Natural, Artificial, Shadowy
	Background Complexity	Plain, Cluttered, Natural Habitat
	Presence of Humans	None, Nearby, Interacting
	Animal Activity State	Resting, Moving, Feeding, Playing
	Occlusions	Fully Visible, Partially Hidden
CELEBA	Weather Conditions	Sunny, Cloudy, Rainy, Foggy, Snowy
	Seasonal Variations	Summer Coat, Winter Coat, Shedding Fur
CELEBA	Gender	Male, Female
	Age	Child, Teenager, Adult, Elderly
	Facial Expression	Neutral, Smiling, Frowning, Surprised
	Hairstyle	Short, Long, Bun, Braided
	Hair Color	Black, Brown, Blonde, Red
	Skin Tone	Light, Medium, Dark
	Facial Hair	Beard, Mustache, Clean-shaven
	Presence of Accessories	Glasses, Earrings, Necklace
	Lighting Conditions	Bright, Dim, Shadowed
	Makeup	Natural, Heavy, None
CIFAR-10	Size	Large, Medium, Small
	Pose/Orientation	Side View, Top View, Angled
	Lighting	Daylight, Nighttime, Shadows
	Background Complexity	Plain, Crowded
	Object Occlusion	Partially Visible, Fully Visible
GTSRB	Shape of Sign	Round, Triangular, Rectangular
	Color of Sign	Red, Blue, Yellow, White
	Size of Sign	Small, Medium, Large
	Weather Conditions	Sunny, Rainy, Foggy, Overcast
	Lighting	Daylight, Nighttime, Shadows, Glare
WaterBirds	Surrounding Environment	Forest Floor, Beach, Lake, River, Ocean, Shoreline
	Background Elements	Trees, Bushes, Rocks, Water Bodies, Sand, Human-made Structures
	Lighting Conditions	Full Daylight, Shaded Areas, Low-light, Overcast
	Weather Conditions	Sunny, Cloudy, Rainy, Foggy, Windy

1034 **G.2 Attribute-Value Annotation**

1035 We employ Llama 3.2 [78], a Vision-Language Model (VLM) with 11B parameters, to determine the most
 1036 suitable value among a set of possible attributes and values for a given dataset. By iterating over a set of images
 1037 in the validation set, the VLM generates metadata, which is subsequently utilized to identify the spurious
 1038 features. Each image approximately takes 4-10 seconds on average to annotate, depending on the size of the
 1039 image. The system prompt provided to Llama 3.2 is as follows:

1040
 1041 *You are an expert in identifying visual attributes in a given image. You will be presented with an im-
 1042 age along with attributes and a list of choices for each of the attributes. You will be asked to choose the most
 1043 suited choice for each of the attributes present in the image. Only choose one choice among all given choices*

1044 for a particular attribute. Ensure that the choice is a string. Reproduce the attribute and the choice as it is.
1045 Preserve the case and the spelling. Respond with only a valid JSON object with the attributes as the keys and the
1046 chosen choices as the values, and no other extra fluff. Use double inverted commas.

1047 **H Training Procedure**

1048 **H.1 Model Configuration and Metrics**

1049 We maintained consistent hyperparameter settings across all baselines, with the only variation being the subset
1050 of training data selected by each method. The validation set was used to identify underlying spurious biases, as
1051 outlined in Section 3.2. For baseline comparisons, we utilized publicly available implementations. In cases where
1052 the code was not open-sourced or experiments were not conducted on the specific datasets, we implemented
1053 the methods and used the respective datasets for evaluation. For TracIN, we employed the fast implementation
1054 available in the Captum library [104].

1055 Since many real-world datasets lack well-defined group structures [17], which are typically needed for evaluating
1056 worst-group accuracy, we compare our method and baselines primarily on average accuracy. Additionally, to
1057 understand the influence of deleting data samples in mitigating spurious features, we follow the experiment
1058 setup defined by [28, 29, 17] and analyze the worst-case performance improvement. We used the methodology
1059 proposed in [43] to create a subset of CELEBA with specific simplicity biases.

1060 **H.2 Model Training and Datasets**

1061 All experiments reported in Table 1 were conducted using the ResNet-18 architecture. The models were trained
1062 from scratch with random initialization. For the WaterBirds dataset, the classifier was trained for 15 epochs
1063 using stochastic gradient descent with a momentum value of 0.9 and a learning rate of 0.001. For all other
1064 datasets, we used the Adam optimizer with a learning rate of 0.001.

1065 The AWA2-A, AWA2-B, CELEBA, models were trained for 15 epochs, while the GTSRB and CIFAR-10 models
1066 were trained for 5 epochs. We have used the same 10 classes as mentioned in Boecking et al. [105] for all
1067 experiments related to AWA2. For CELEBA, we used a subset of 10,000 examples from the original dataset,
1068 with the target label being hair color (blond) and the spurious feature being gender (male). Additionally, we
1069 induced a spurious correlation of 0.4 between the target and spurious features to mimic real-world biases. For
1070 experiments related to ImageNet-100, we have considered the subset of the ImageNet dataset with 100 classes as
1071 per Tian et al. [91] and trained the model for 10 epochs with the Adam optimizer. We have further considered
1072 the attributes related to texture and shape for common classes available for the ImageNet dataset [106]. The
1073 cutoff value to mark an attribute-value pair as spurious (τ) was decided based on the size of the corresponding
1074 pair in the validation dataset, and the pair generating the largest difference with respect to the original dataset
1075 was picked for analysis.

1076 To ensure a fair comparison for subset selection, we maintained uniformity in the training process across both
1077 the original model training and the retraining process after data deletion.

1078 The experiments reported in Table 3, Table 4 were conducted using the ResNet-18 model, trained for 10 epochs
1079 with the Adam optimizer and a learning rate of 0.001. The dataset was created by randomly sampling the
1080 correlation factor within the range [0,1] and varying the training data size across [5000, 3000, 7000, 10000]. The
1081 correlation attribute and target attribute were selected from the metadata provided in the CELEBA dataset [43].
1082 Experiments on the following target-correlated attribute pairs—(arched eyebrows, receding hairline), (attractive,
1083 mouth slightly open), (big nose, male), (goatee, bushy eyebrows), (mouth slightly open, smiling), (mouth slightly
1084 open, wearing lipstick), (narrow eyes, eyeglasses), (pointy nose, mouth slightly open), (receding hairline, rosy
1085 cheeks), and (male, pointy nose) are conducted with varying training dataset sizes of 3000, 5000, 5000, 5000,
1086 5000, 5000, 7000, 7000, 7000, and 5000 samples respectively, and corresponding spurious correlation strengths
1087 of 0.2, 0.8, 0.4, 0.4, 0.8, 0.9, 0.2, 0.6, 0.6, and 0.6 respectively. Further experiments on the target attributes
1088 Bangs, Big Nose, Heavy Makeup, and Wearing Earrings, were conducted with correlation factors of 0.6, 0.2,
1089 0.4, and 0.2, and with training sample sizes of 10000, 5000, 3000, and 5000, respectively. Results for these
1090 experiments are provided in Table 14

1091 **H.3 Data Attribution**

1092 For the experiments reported in Table 1, approximately 3% of the data was removed from the training dataset.
1093 We fix the data removal budget across all baselines, as it is a design choice best left to domain experts. A
1094 smaller removal percentage prevents overpruning of the dataset (training sample for group land bird on water
1095 is around 56 out of 4795 [29]) and highlights the precision of attribution methods by focusing on the most
1096 harmful samples. In contrast, larger removals can obscure differences between methods due to overlapping
1097 sample selections. For experiments related to spurious correlation in celeba, considering the stochasticity of the

1098 training sample, we have fixed the budget size to 100 samples. Further ablation on subset size is provided in
1099 Appendix Q.1. We ensured uniformity in the data deletion process by basing it on the validation attribution score
1100 \mathcal{A} , calculated according to the respective definition of data attribution α in each baseline method, using their
1101 default hyperparameters.

1102 For our proposed method, we performed hyperparameter tuning by selecting the rank parameter (t) from [50, 40,
1103 10, 100] and the minimum weight (β) from [0.6, 0.7, 0.8, 0.9, 0.95]. The weight barrier (C) was chosen from
1104 [5, 10]. The optimization for Equation 10 was performed for 5000 iterations using the Adam optimizer with a
1105 learning rate of 0.0001. The value of γ is decided based on the fraction of the dataset that is removed from the
1106 training dataset. For experiments reported in Table 3 and Table 4, hyperparameter tuning was performed over
1107 the same range as in previous experiments, optimizing for both best average performance and best worst-group
1108 accuracy separately.

1109 **H.4 Textual Description**

1110 For different datasets, we used distinct textual representations of the underlying bias. The choice of textual
1111 descriptions in our experiments depends not only on the attribute-value pairs but also on the dataset itself. For
1112 instance, datasets like AWA2-A contain only label-specific information, such as color and habitat type, without
1113 an explicit attribute-value format. Therefore, a suitable textual representation for this dataset could be "*It is a*
1114 *(*1) animal.*" Here, (*1) represents the feature identified as a potential biased candidate. Similarly, for GTSRB,
1115 incorporating dataset context improves model performance, and a possible template could be "*(*1) of the sign is*
1116 *(2).*" where (*1) and (2) are replaced by the corresponding attribute and value pair.

1117 For datasets such as WaterBirds, AWA2-A, AWA2-B, CELEBA, GTSRB, CIFAR-10, and ImageNet-100 the
1118 textual descriptions used in the experiments related to Table 1 are provided in Table 10:

Table 10: Textual Descriptions of Spurious Feature for Different Datasets

Attribute Description	Dataset
<i>Surrounding environment in image is forest floor</i>	WaterBirds
<i>It is a domestic animal</i>	AWA2-A
<i>Size of the animal is very large</i>	AWA2-B
<i>Image of a male with blond hair</i>	CELEBA
<i>Shape of the sign is round</i>	GTSRB
<i>Size of the entity is large</i>	CIFAR-10
<i>Object has a spotted pattern</i>	ImageNet-100

1119 For all experiments related to Table 3, Table 4, we used a standardized textual format: "*Image of a person with*
1120 *(*1) and (2).*" where (*1) and (2) correspond to the target class and the correlated attribute, respectively. Further
1121 experiments using VLM-based textual description in Table 5 for the target attributes Wearing Earrings, Bangs,
1122 Big Nose, Heavy Makeup use textual description as "*Person is wearing glasses*", "*Image of a male person*",
1123 "*Person has long hair*", and "*Person is wearing glasses*" respectively. For metadata, we used the same format as
1124 the Table 3.

1125 **I Comparison with Other Optimization and Data-Centric Methods**

1126 In general, ImageNet initialization [107] plays a crucial role in achieving strong worst-group accuracy. However,
1127 most of our experiments are conducted without ImageNet pretraining to better reflect practical deployment
1128 scenarios, particularly those where spurious correlations can significantly degrade model performance [107]. For
1129 a fair comparison with optimization-based methods such as gDRO [17] and JTT [16], we additionally evaluate
1130 our method on the Waterbirds dataset using a ResNet-18 model pretrained on ImageNet, along with LLM-
1131 generated attribute-value annotations. Results averaged over three independent runs are reported in Table 11.
1132 We also include comparisons with data deletion methods like D3M [11] and group-balancing approaches such as
1133 SUBG and RWG [29].

1134 Table 11 compares the average and worst-group accuracy of our method against various robustness-based
1135 approaches on the Waterbirds dataset. Methods are grouped based on whether they require group annotations for
1136 the entire training dataset and whether they support textual bias descriptions.

1137 Our method achieves a competitive average accuracy (0.855) and strong worst-group accuracy (0.756) without
1138 relying on group annotations, while uniquely supporting textual bias descriptions. Compared to other methods
1139 like ERM, D3M, and JTT, our method improves worst-group accuracy by +27.9% over ERM, +12% over JTT,

1140 and +1.6% over D3M. Further comparison with D3M with the same training setup as Table 3 is provided in
1141 Table 6.

1142 Group annotation-based methods like gDRO and RWG perform best on worst-group accuracy, but at the cost of
1143 requiring explicit group labels for the entire training dataset.

1144 Additional challenges associated with these methods in specific applications are discussed in Section 1, Sec-
1145 tion 2.2 and Appendix E.

Table 11: Comparison of Average Accuracy and Worst group accuracy achieved by our method in
comparison with other robustness-based methods on Waterbirds.

Method	Group Annotation (Train)	Supports Textual Bias Description	Average Accuracy	Worst Group Accuracy
ERM	\times	\times	0.819	0.477
D3M	\times	\times	0.903	0.740
JTT	\times	\times	0.852	0.636
Ours	\times	\checkmark	0.855	0.756
RWG	\checkmark	\times	0.864	0.822
SUBG	\checkmark	\times	0.833	0.814
gDRO	\checkmark	\times	0.886	0.836

J Empirical Validation of Theoretical Formulation

1147 To validate our theoretical claim, we used the codebase provided by Eyuboglu et al. [43] to sample a 10k subset
1148 from CELEBA, where the attributes Male and Smiling are highly correlated. We then computed Trak scores
1149 for the training dataset using a ResNet-18 classifier trained to predict the Male label. In this setting, due to the
1150 strong correlation between Male and Smiling [43, 108] , smiling may act as a spurious feature. Since the task is
1151 to distinguish males from females, we consider features like Beard and Moustache to be more causally relevant,
1152 and thus expect that samples with these features to have lower \mathcal{A} scores compared to those with Smiling.

1153 However, statistical analysis of the detrimental attribution(\mathcal{A}) scores using T-test for the training samples reveals
1154 that Smiling has lower scores for samples compared to samples with Beard and Moustache (Table 12). The
1155 difference is statistically significant for Beard ($p < 0.001$). This supports Proposition 1, demonstrating that such
1156 effects can arise in practical scenarios.

Table 12: Mean and standard deviation of detrimental attribution ($|\mathcal{A}|$) scores for different attributes,
along with statistical significance from a two-sample t-test against *Smiling*.

Attribute	Mean	Std	p-value (vs Smiling)	Significance
Smiling (spurious)	0.539	0.056	—	—
Moustache	0.545	0.044	0.1008	Not significant
Beard	0.544	0.036	0.00039	Significant

K Worst Class Performance

1157 Table 13 reports gains in the worst-performing class for each dataset. In Awa2-A and Awa2-B, worst-class
1158 accuracy more than doubles, while in GTSRB, it improves from 50% to 70%. These results demonstrate that our
1159 method enhances class-level performance with minimal negative impact on other classes.

Table 13: Worst-class accuracy before and after retraining. The table shows the original worst-class
accuracy and the corresponding value after retraining with spurious samples removed.

Dataset	Original Worst-Class Accuracy	Retrained Worst-Class Accuracy
Awa2-A	0.040	0.103
Awa2-B	0.040	0.103
CIFAR-10	0.589	0.575
GTSRB	0.500	0.700
ImageNet-100	0.100	0.100

1161 L Group-wise Accuracy Improvements

Table 14: Comparative evaluation of the proposed method (Ours) with the full training baseline (Original) and Trak, reporting the best average and best worst group accuracy (mean_{std}) across three runs.

Target Attribute	Spurious Attribute	Average Accuracy			Worst Group Accuracy		
		Original	Trak	Ours	Original	Trak	Ours
Bangs	Black Hair	0.920 _{0.007}	0.921 _{0.006}	0.923 _{0.006}	0.523 _{0.079}	0.571 _{0.053}	0.649 _{0.049}
Big Nose	Wearing Necklace	0.765 _{0.032}	0.787 _{0.009}	0.787 _{0.010}	0.127 _{0.065}	0.080 _{0.047}	0.347 _{0.148}
Heavy Makeup	Straight Hair	0.805 _{0.031}	0.800 _{0.055}	0.826 _{0.024}	0.651 _{0.137}	0.686 _{0.078}	0.716 _{0.088}
Wearing Earrings	Bags Under Eyes	0.791 _{0.020}	0.792 _{0.019}	0.798 _{0.028}	0.040 _{0.029}	0.017 _{0.029}	0.281 _{0.170}

1162 Table 15 presents group-wise accuracy before and after removing samples associated with spurious features
1163 associated with Table 14. Groups 1–4 show baseline performance, while Groups 1*–4* report results after
pruning. Our method yields notable improvements in some groups without major drops in others.

Table 15: Group-wise accuracy before and after removing spurious samples. The table reports the mean accuracy and standard deviation over 3 runs. Groups 1–4 represent the training with the original dataset, while Groups 1*–4* correspond to results after data pruning.

Target Attr	Spurious-Attr	G1	G2	G3	G4	G1*	G2*	G3*	G4*
Bangs	Black Hair	0.73 _{0.07}	0.97 _{0.02}	0.53 _{0.08}	0.98 _{0.01}	0.78 _{0.06}	0.96 _{0.01}	0.59 _{0.12}	0.97 _{0.01}
Big Nose	Necklace	0.13 _{0.06}	0.94 _{0.04}	0.32 _{0.11}	0.89 _{0.07}	0.22 _{0.09}	0.94 _{0.03}	0.37 _{0.11}	0.89 _{0.06}
Heavy Makeup	Straight Hair	0.68 _{0.14}	0.80 _{0.12}	0.81 _{0.08}	0.82 _{0.07}	0.72 _{0.11}	0.83 _{0.02}	0.80 _{0.06}	0.80 _{0.02}
Earrings	Bags Under Eyes	0.09 _{0.04}	0.99 _{0.01}	0.04 _{0.03}	0.99 _{0.01}	0.28 _{0.17}	0.96 _{0.03}	0.32 _{0.16}	0.91 _{0.07}

1164

1165 M Ablation of Different Components

1166 The ablation study in Table 16 highlights the contribution of key components i.e, data Attribution and CLIP, to
1167 the overall performance of our method. For the given experiment, we have used cosine similarity with CLIP
1168 (Only CLIP) representation to remove samples that align with the description of the underlying bias. When used
1169 independently, both components provide noticeable improvements over the full training baseline, particularly
1170 in average accuracy. However, they exhibit limitations in worst-group accuracy when applied in isolation.
1171 Notably, combining both Attribution and CLIP in our full method yields the highest performance across nearly
1172 all settings, especially in worst-group accuracy, demonstrating the complementary strengths of these components
in addressing spurious correlations.

Table 16: Comparative evaluation of the proposed method (Ours) with the full training baseline (Original), Only Attribution, and Only CLIP, reporting the best average and best worst group accuracy (mean_{std}) across three runs.

Target Attribute	Spurious Attribute	Average Accuracy			Worst Group Accuracy			
		Original	Only Attribution	Only CLIP	Ours	Original	Only Attribution	Only CLIP
Bangs	Black Hair	0.920 _{0.007}	0.921 _{0.006}	0.922 _{0.008}	0.923 _{0.006}	0.523 _{0.079}	0.571 _{0.053}	0.649 _{0.049}
Big Nose	Wearing Necklace	0.765 _{0.032}	0.787 _{0.009}	0.777 _{0.002}	0.787 _{0.010}	0.127 _{0.065}	0.080 _{0.047}	0.347 _{0.148}
Heavy Makeup	Straight Hair	0.805 _{0.031}	0.800 _{0.055}	0.813 _{0.010}	0.826 _{0.024}	0.651 _{0.137}	0.686 _{0.078}	0.739 _{0.045}
Wearing Earrings	Bags Under Eyes	0.791 _{0.020}	0.792 _{0.019}	0.791 _{0.021}	0.798 _{0.028}	0.040 _{0.029}	0.017 _{0.029}	0.281 _{0.170}

1173

1174 N Architecture-based Ablation on Worst Group Accuracy and Average Accuracy

1176 We further evaluate our method on the WaterBirds dataset across different architectures, including ResNet-
1177 18, VGG16, VGG13, AlexNet, and ConvNet. Pham et al. [107] shows that the random initial weights can
1178 significantly impact the worst group performance of a model, especially in smaller networks. To replicate this
1179 setting, we tested our method under extreme conditions, maintaining consistency in textual instructions and
1180 using a single run with the same random seed across all baselines.

1181 As shown in Table 18 and Table 17, In comparison with the complete data setting our method achieves an
1182 improvement of 5.0%, 1.9%, 3.6%, 3.1%, 12.6% in worst-group accuracy for VGG16, VGG13, Convnet,
1183 ResNet18 and AlexNet architecture and an improvement of 5.2%, 7.1% 4.9% and 7.1% for VGG16, ConvNet,
1184 ResNet18, and AlexNet in average accuracy respectively.

1185 Furthermore, compared to Trak, our method achieves an improvement of 1.1%, 2.4%, and 4.8% in average group
 1186 performance for ConvNet, ResNet18, and AlexNet, respectively. Additionally, enhancements of 5.0%, 1.4%,
 1187 7.8%, 4.5%, and 12.9% in worst-group performance were observed for VGG16, VGG13, ConvNet, ResNet18,
 1188 and AlexNet.

Table 17: Architecture Ablation on WaterBirds (Best Worst Group Accuracy)

Model	Original	Random	IF	TracIN	EWC	Trak	Ours
VGG16	0.053	0.050	0.064	0.064	0.062	0.053	0.103
VGG13	0.048	0.053	0.087	0.030	0.065	0.053	0.067
ConvNet	0.090	0.034	0.064	0.033	0.053	0.048	0.126
ResNet18	0.050	0.064	0.067	0.017	0.048	0.036	0.081
AlexNet	0.050	0.048	0.107	0.031	0.042	0.047	0.176

Table 18: Architecture Ablation on WaterBirds (Best Average Accuracy)

Model	Original	Random	IF	TracIN	EWC	Trak	Ours
VGG16	0.640	0.669	0.657	0.640	0.683	0.686	0.692
VGG13	0.655	0.640	0.610	0.668	0.660	0.669	0.662
ConvNet	0.654	0.705	0.640	0.721	0.711	0.714	0.725
ResNet18	0.641	0.604	0.600	0.694	0.623	0.666	0.690
AlexNet	0.644	0.650	0.586	0.693	0.658	0.667	0.715

1189 O Experiment on Vision Transformer

1190 Existing data attribution methods typically compute gradients over all model parameters, which often causes
 1191 memory issues for large models like Vision Transformers. To address this, we follow recent works [104, 58] and
 1192 calculated the gradients only for the final feature layer for both Trak and our method. However, this adaptation
 1193 was incompatible with other baselines.

1194 The results on Waterbirds for both methods are shown in Table 19.

Table 19: Best Average Accuracy and Best Worst Group performance analysis of our method in
 comparison with Trak and Original training of vision transformer with entire dataset.

	Average Accuracy	Worst Group Accuracy
original	0.601/0.000	0.104/0.000
Trak	0.644/0.020	0.0740/0.014
ours	0.640/0.027	0.1671/ 0.014

1195 P Relative Comparison with the Baselines

1196 For experiments related to Table 14, we have provided a comparison of the relative performance improvement
 1197 achieved by our method against other baselines over the complete training data setting. As shown in Table 20
 1198 and Table 21, our method, on average, outperforms other baselines in terms of best average accuracy and best
 1199 worst group accuracy.

Table 20: Relative improvement in Best Average Accuracy (%) achieved by our method and other
 baselines compared to the complete data setting(Original). The results represent the mean scores
 from three independent runs, with the best-performing values highlighted in **bold**.

Target Attribute	Spurious Attribute	Random	EWC	IF	TracIN	Trak	Ours
Bangs	Black Hair	-0.03	0.37	0.36	-0.07	0.16	1.05
Big Nose	Wearing Necklace	-0.07	1.66	1.10	-0.17	2.23	2.17
Heavy Makeup	Straight Hair	-0.44	-1.05	0.95	-2.83	-0.44	2.18
Wearing Earrings	Bags Under Eyes	0.3	-0.2	-1.17	-0.57	0.1	0.73

Table 21: Relative improvement in Best Worst Group Accuracy (%) achieved by our method and other baselines compared to the complete data setting(Original). The results represent the mean scores from three independent runs, with the best-performing values highlighted in **bold**.

Target Attribute	Spurious Attribute	Random	EWC	IF	TracIN	Trak	Ours
Bangs	Black Hair	6.25	15.62	6.66	7.05	4.77	12.58
Big Nose	Wearing Necklace	4.4	-3.57	5.10	4.68	-4.65	22.08
Heavy Makeup	Straight Hair	1.84	5.95	4.30	-1.24	3.55	6.54
Wearing Earrings	Bags Under Eyes	5.93	1.53	13.54	-3.46	-3.23	24.17

1200 Q Sensitivity Analysis

1201 Table 22 and Table 23 show the sensitivity of our proposed method on different hyperparameter values.

Table 22: Sensitivity analysis of the average accuracy of our method on the WaterBirds dataset for hyperparameters like the barrier constant (C), the matrix rank (t) (shown by rows), and the minimum weight fraction (β , shown by columns).

Barrier (C)	Rank (t)	0.6	0.7	0.75	0.8	0.85	0.9
5	40	0.657	0.619	0.648	0.673	0.650	0.640
	50	0.673	0.642	0.621	0.618	0.618	0.601
	100	0.670	0.678	0.650	0.602	0.632	0.631
10	40	0.690	0.671	0.615	0.634	0.621	0.650
	50	0.633	0.679	0.639	0.657	0.629	0.609
	100	0.653	0.663	0.602	0.642	0.660	-

Table 23: Sensitivity analysis of the worst group accuracy of our method on the WaterBirds dataset for hyperparameters like the barrier constant (C), the matrix rank (t) (shown by rows), and the minimum weight fraction (β , shown by columns).

Barrier (C)	rank (t)	0.6	0.7	0.75	0.8	0.85	0.9
5	40	0.037	0.051	0.042	0.020	0.050	0.041
	50	0.033	0.042	0.055	0.048	0.056	0.065
	100	0.020	0.036	0.041	0.081	0.041	0.050
10	40	0.009	0.037	0.056	0.051	0.044	0.030
	50	0.044	0.023	0.053	0.031	0.051	0.061
	100	0.045	0.031	0.065	0.034	0.034	-

1202 Q.1 Performance Analysis on Different Subset Size

1203 To further analyze model performance across different subset sizes, we conducted an ablation study where the
1204 best hyperparameters were kept fixed while varying the proportion of removed training data. The results are
1205 summarized in Table 24.

Table 24: Sensitivity analysis of the worst group accuracy and average accuracy of our method on the WaterBirds dataset for different subset sizes.

Metrics	3%	5%	15%	25%
Average Accuracy	0.69	0.645	0.682	0.712
Worst group Accuracy	0.081	0.041	0.037	0.002

1206 R Time Taken for Subset Selection

1207 In Figure R, we compare the time taken by our method in comparison with other baselines to select a subset of
1208 1200 images from 60,000 images of CIFAR-10 for the instruction mentioned in Table 10. Since our method uses
1209 the attribution scores generated by Trak and improves upon it. The time taken by our method is slightly longer
1210 than Trak.

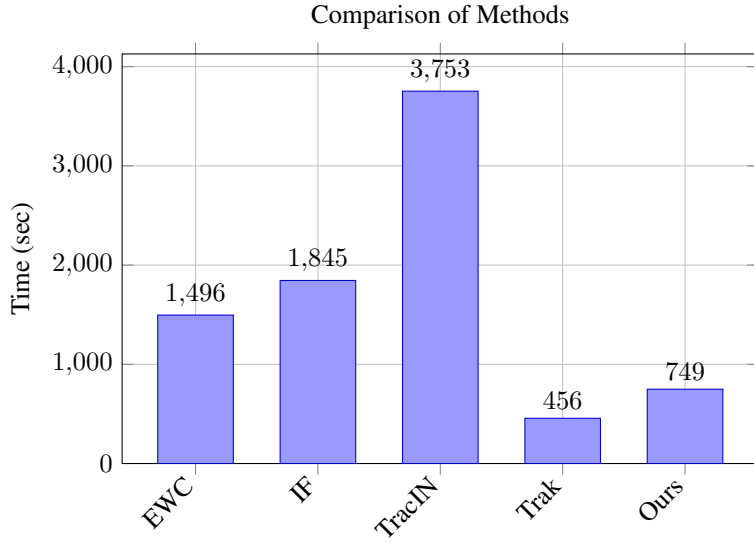


Figure 2: Comparison of time taken to select a subset of 1200 samples from a training dataset of 60,000 images of CIFAR-10 by different baselines and (Ours) for a given textual instruction.

1211 **S Memory Consumption and Other Training Overhead**

1212 The Table 25 reports GPU and RAM usage of our method compared to other baselines, using the same setup
 1213 described in Appendix R.

1214 As shown, our method introduces only a marginal computational overhead over Trak, which we use for computing
 1215 data attribution scores. It is to be noted that, while Trak is more memory-intensive, it produces better linear
 1216 datamodeling score (LDS) scores than other baselines [32].

Table 25: GPU and RAM utilization (in MB) of our method compared to baseline approaches.

Method	GPU Memory (MB)	RAM Usage (MB)
IF	27,749	10,578
EWC	13,221	10,520
TracIN	44,087	9,629
Trak	48,020	10,710
Ours	48,525	10,722

1217 **T Workflow**

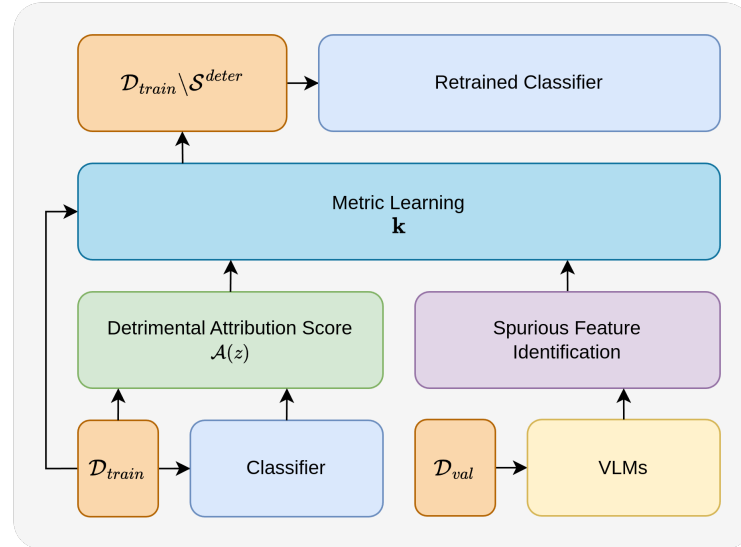


Figure 3: Diagram depicting the workflow of the proposed method

1218 **U Images**

1219 In this section, we have shown the images that have been removed from the training dataset. Figure 4, Figure 5,
1220 Figure 6, and Figure 7 show the set of images that have been removed by our method from the training dataset
1221 as (S^{deter}) . For WaterBirds, GTSRB, CELEBA, and AWA2-B, respectively.



Figure 4: Set of images removed by our method for WaterBirds. The instruction set used for this experiment is “*The surrounding environment in the image is forest floor*”.



Figure 5: Set of Images removed by our method for GTSRB. The instruction set used for this experiment is “*Shape of sign is round.*”

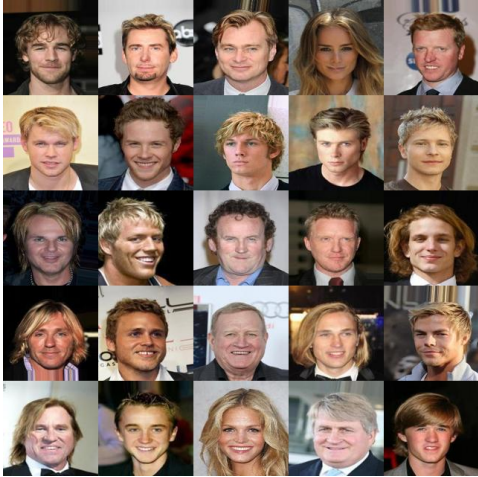


Figure 6: Set of Images removed by our method for CELEBA. The instruction set used for this experiment is “*Image of a male with blonde hair*”.



Figure 7: Set of Images removed by our method for Awa2-B. The instruction set used for this experiment is “*The size of the animal is very large*.”